TISSUEFAXS CYTOMETRY – ENABLING PRECISION MEDICINE

Applications of Tissue Cytometry – Immunophenotyping, Spatial Analysis and Quantification of the Tumor Microenvironment *in-situ*

Rupert C. Ecker
CEO

TG has been member of 5 EU-funded Marie Curie European Training Networks

AID PATH Academia and Industry Collaboration for Digital Pathology

InCeM The European network for cell migration studies www.incem.rwth-aachen.de

ALKATRAS

CaSR CaSR Biomedicine Training Network

HELICAL

THE TISSUEGNOSTICS GROUP

2021: TG celebrates 18th Anniversary!
Installations in 32 countries on 6 continents!

January 2021
* publications from 59 countries
* 1649 reference publications

Headquarter TissueGnostics GmbH
Taborstrasse 10/2/8, 1020 Vienna, Austria

International Offices
TissueGnostics Romania SRL, Iasi, Romania
TissueGnostics USA Inc., Los Angeles & Worcester, MA
TissueGnostics Asia-Pacific, Hong Kong & Beijing

TissueGnostics is ISO certified and products are CE-marked!

1
TG wins 1st place in Image Analysis at the International Scanner Contest 2016

INTERNATIONAL R&D ACTIVITIES

AIDPATH

Academia and Industry Collaboration for Digital Pathology - focused on developing efficient and innovative products for digital pathology.

CaSR-Biomedicine

Innovative Training Network on the **Calcium-sensing receptor (CaSR)**, which is involved in breast cancer, diabetes, asthma and Alzheimer's disease.

ALKATRAS

Tranlational Oncology and research on ALK-related malignancies to develop novel therapies.

InCeM – European Network on Cell Migration

Research on Integrated Component Cycling in Epithelial Cell Motility. Focus on cell migration, a fundamental biological process occurring throughout the human body at any point in life.

HELICAL – BIG Data for Clinical Benefit

Research on Integrated Component Cycling in Epithelial Cell Motility. Focus on cell migration, a fundamental biological process occurring throughout the human body at any point in life.

THE *TISSUEFAXS*™ PRODUCT FAMILY

For histological slides:

TissueFAXS PLUS (= fluorescence and brightfield scanning & analysis)

TissueFAXS Fluo (= fluorescence scanning & analysis)

TissueFAXS Histo (= brightfield scanning & analysis)

THE VIRTUAL SLIDE IN IHC

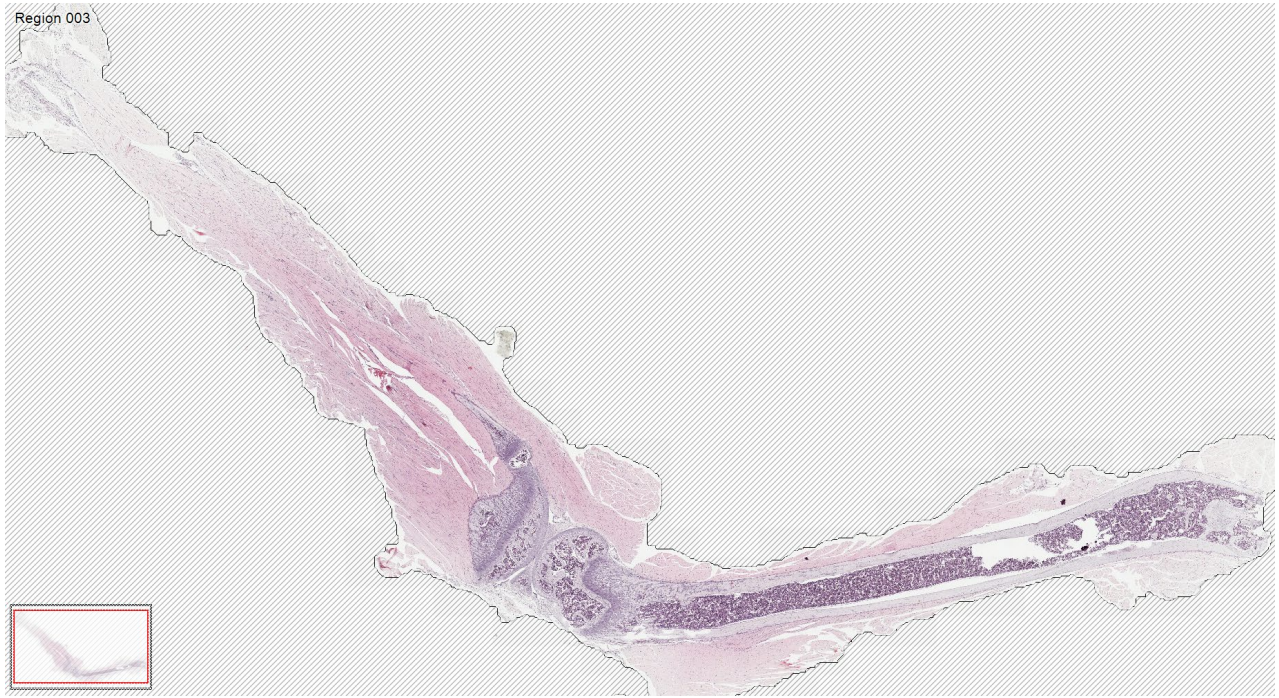

The *digital sample / virtual slide* might consist of thousands of individual fields of view!

Courtesy Dr. Ilaria Belantuono, University of Sheffield, UK

THE VIRTUAL SLIDE IN IHC

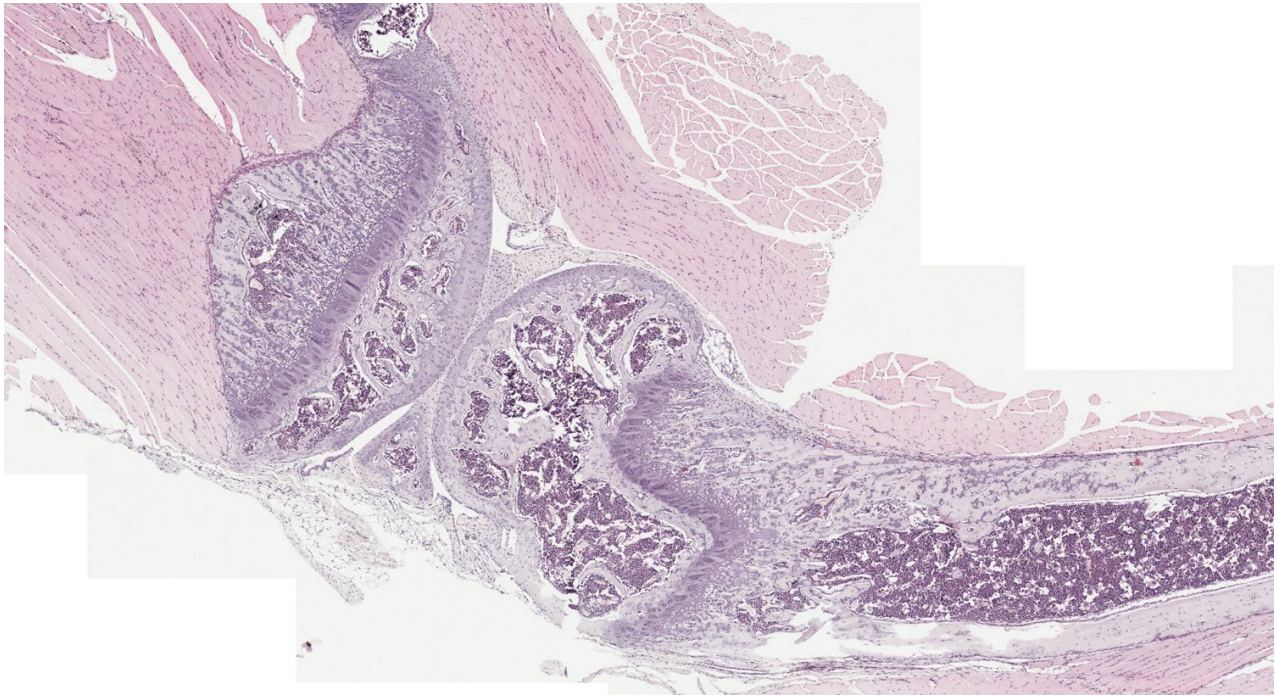

The *digital sample / virtual slide* might consist of thousands of individual fields of view!

Courtesy Dr. Ilaria Belantuono, University of Sheffield, UK

THE VIRTUAL SLIDE IN IHC

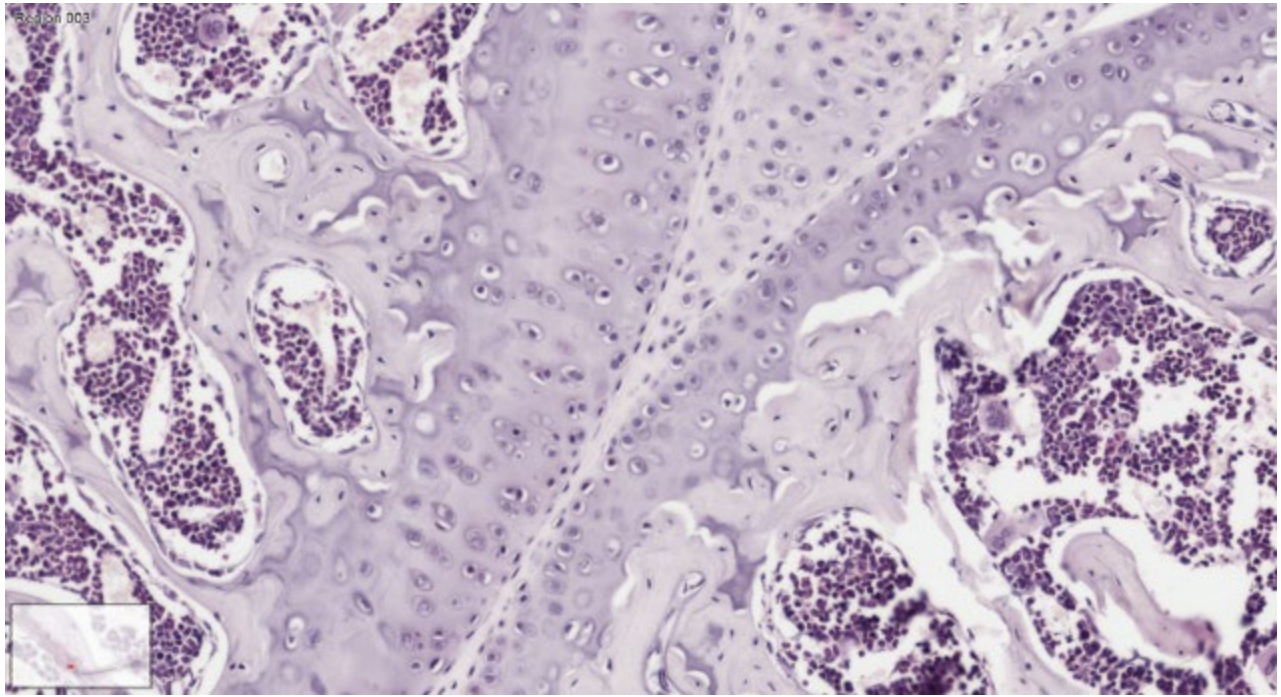

The *digital sample / virtual slide* might consist of thousands of individual fields of view!

Courtesy Dr. Ilaria Belantuono, University of Sheffield, UK

THE *TISSUEFAXS*™ PRODUCT FAMILY

for slides & cell cultures in well-plates

TissueFAXS i PLUS
(= fluorescence and brightfield scanning & analysis)
TissueFAXS i Fluo
(= fluorescence scanning & analysis)
TissueFAXS i Histo
(= brightfield scanning & analysis)

THE *TISSUEFAXS*™ PRODUCT FAMILY

TissueFAXS with spining disc confocal capability:

- Optical sections at high resolution
- Highest image quality
- Analysis of thick tissue sections
- Cytometry of 3D cell cultures
- High scanning speed & cost effectiveness

Available with 8-slide stage upright and inverse systems as well as the SL slide loader (upright only)!

STRATAFAXS II

For histological slides stained with IHC
(= brightfield scanning & analysis)

TISSUE CYTOMETRY SUITE

SQ For contextual tissue cytometry in IF and/or IHC

TQ For histological samples stained with IF (= fluorescence analysis)

HQ For histological samples stained with IHC (= brightfield analysis)

De Novo™ Software

Turning Cytometry Data Into Results

FCS Express 7 Cytometry

QUANTIFICATION OF NUCLEAR MARKERS

TISSUEFAXS™ CYTOMETRY

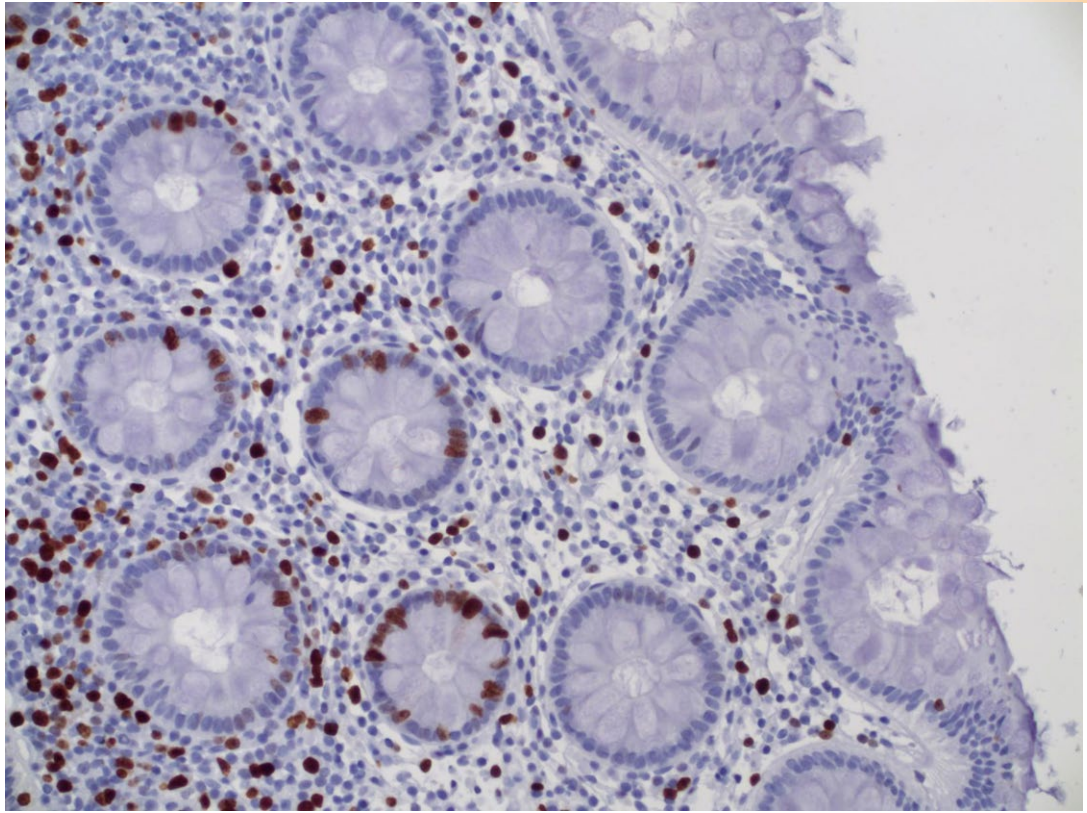

How many of the blue nuclei are also stained in brown (in %)?

Expert‘s estimations:
1% - 40%

TISSUEFAXS™ CYTOMETRY

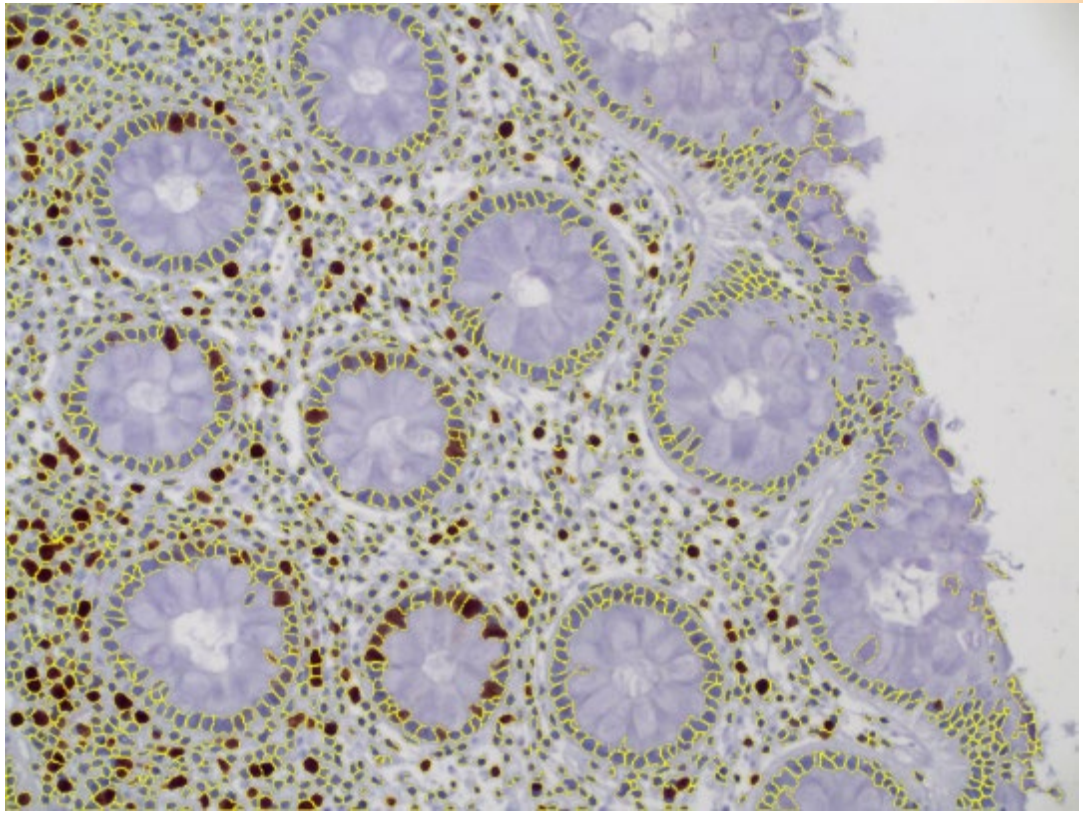

How many of the blue nuclei are also stained in brown (in %)?

Expert‘s estimations:
1% - 40%

TISSUEFAXS™ CYTOMETRY

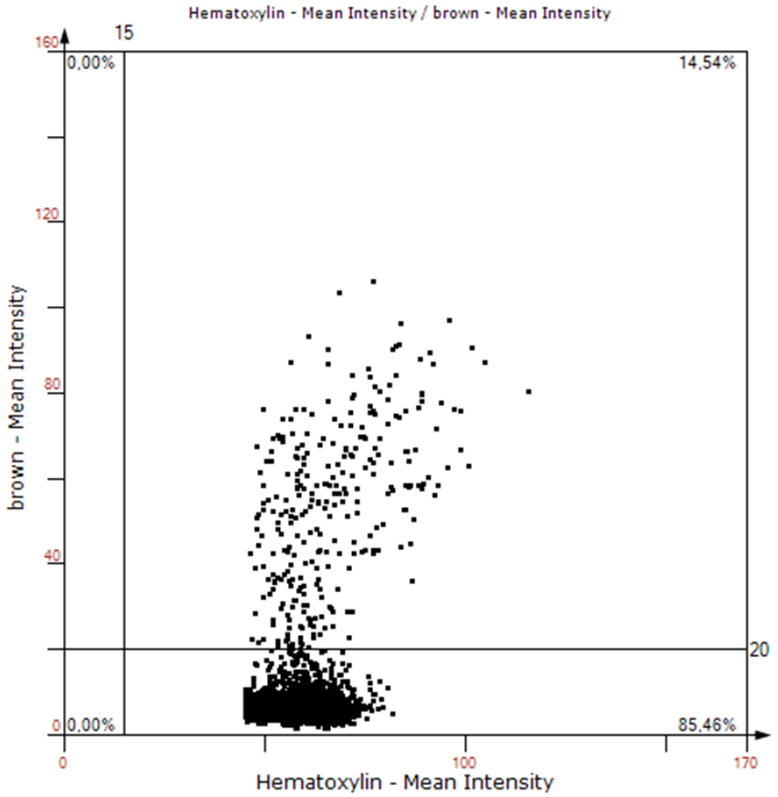

How many of the blue nuclei are also stained in brown (in %)?

Expert‘s estimations:
1% - 40%

Observer independent measurement: 14.54%

QUANTIFICATION OF CELLULAR COMPARTMENTS

CYTOPLASMIC MARKERS

Normal skin

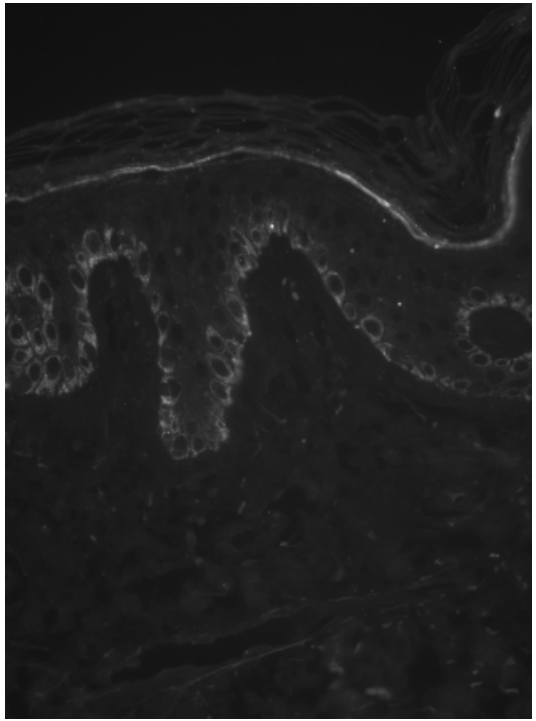

UV-irradiated skin

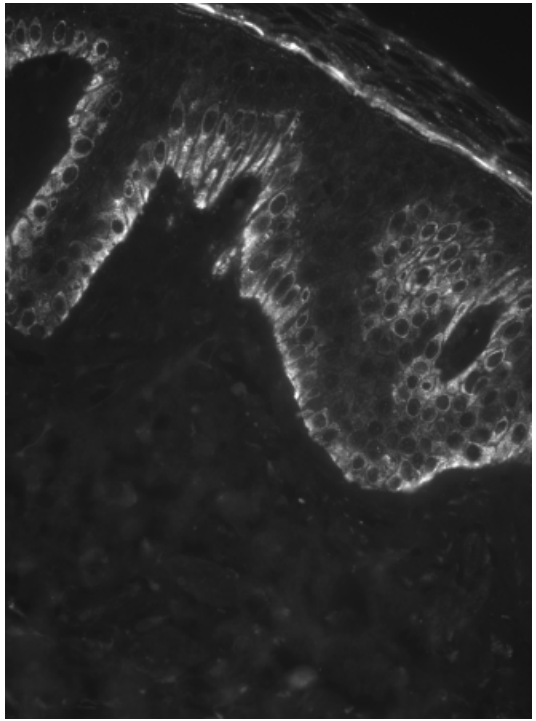

Control mAb

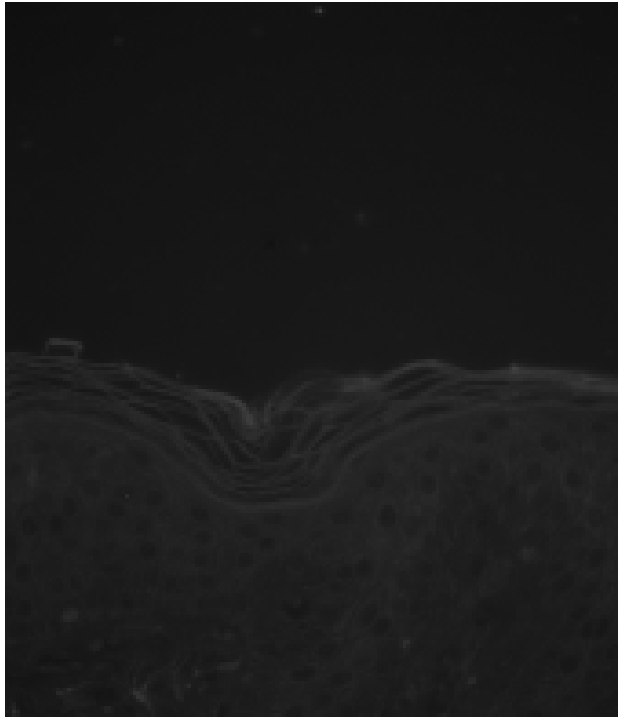

CYTOPLASMIC MARKERS

Each cell is indicated as one dot
The reactivity of two channels is plotted on the x- and y-axes

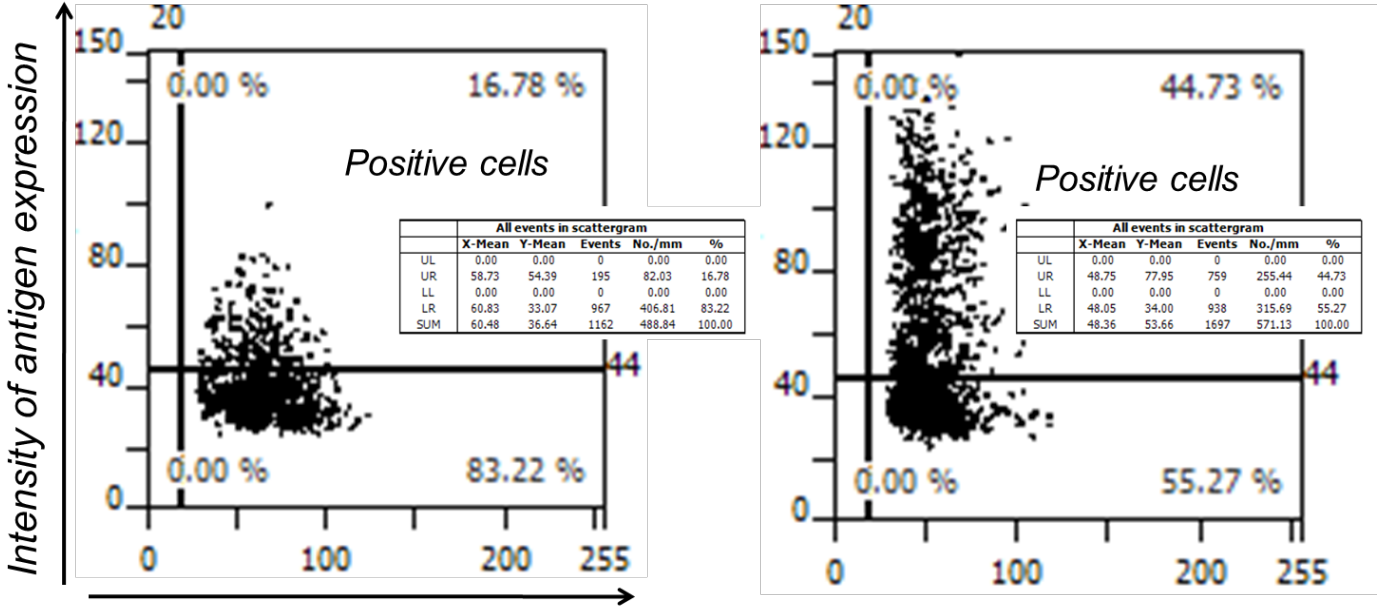

FORWARD CONNECTION

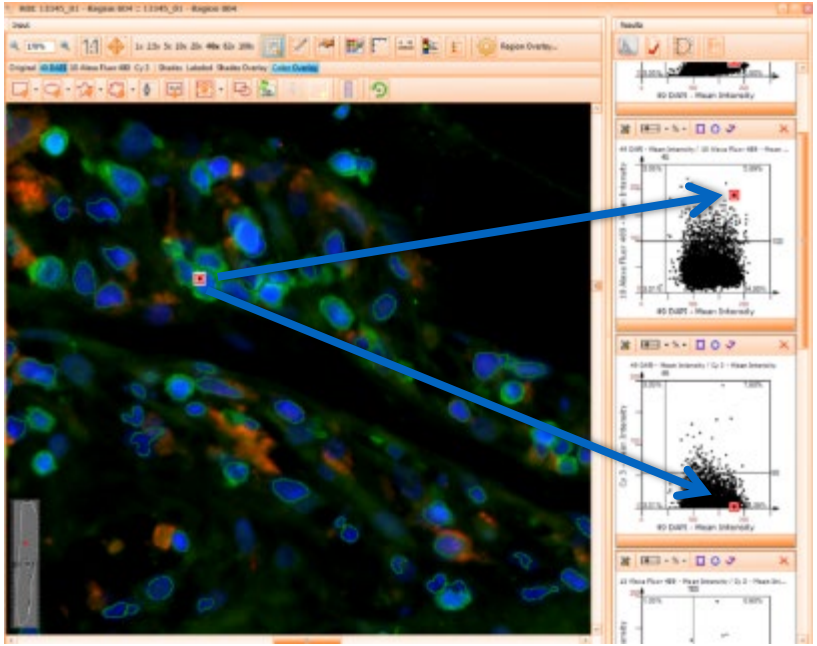

GREEN positive
RED negative

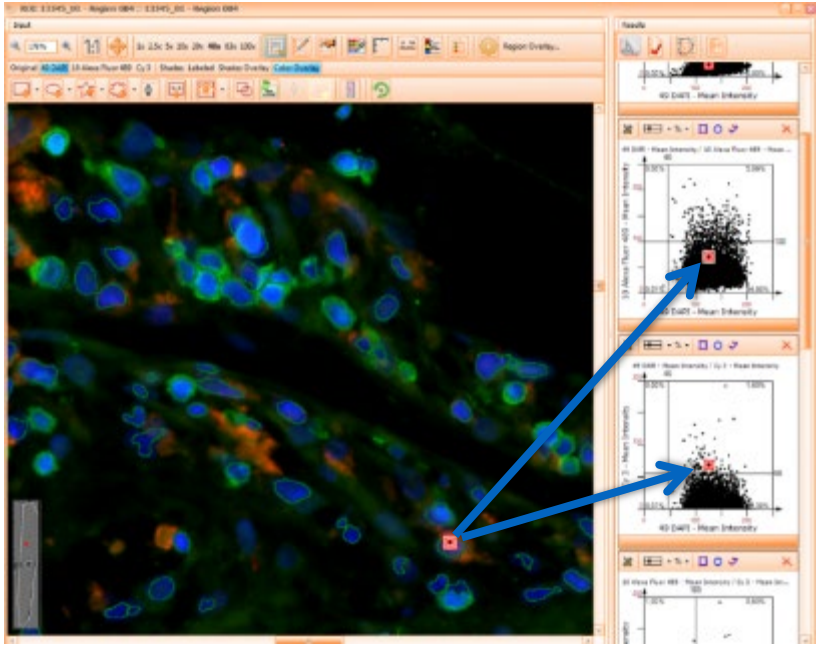

GREEN negative
RED positive

BACKWARD CONNECTION

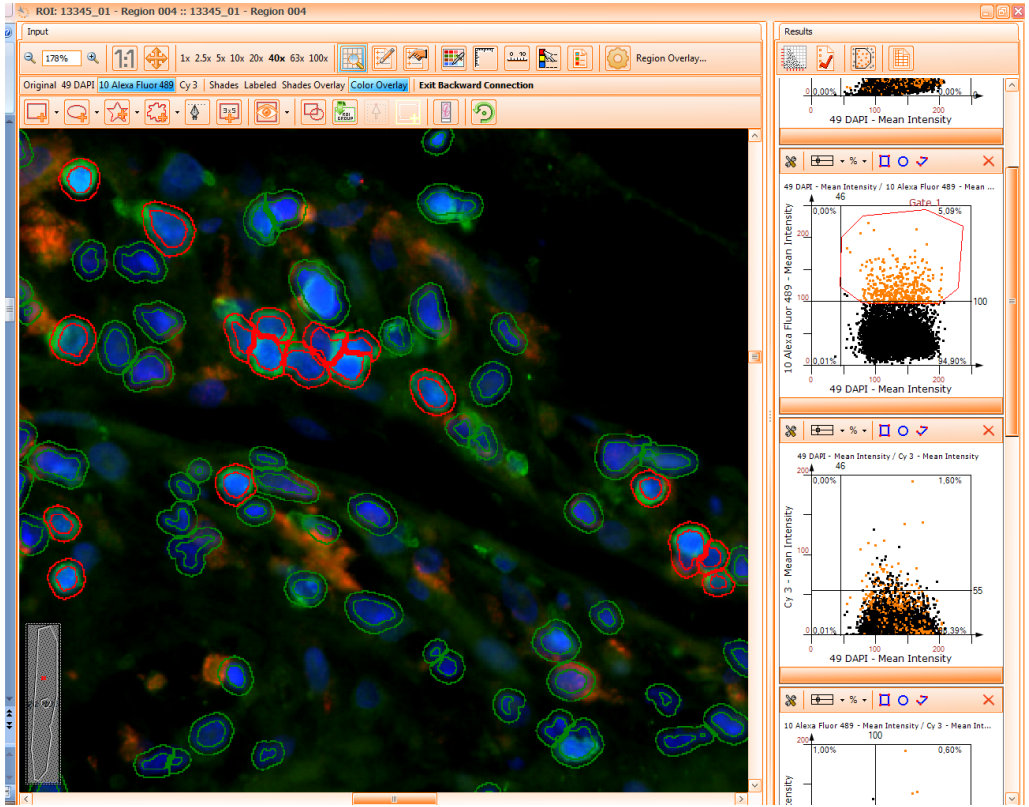

Cells with red contours belong to the highlighted Gate.

TISSUEGNOSTICS
PRECISION THAT INSPIRES

PHENOTYPIC CHARACTERIZATION OF TISSUE-INFILTRATING LEUKOCYTES

APPLICATION NOTE:
PHENOTYPE OF TISSUE INFILTRATING LEUKOCYTES

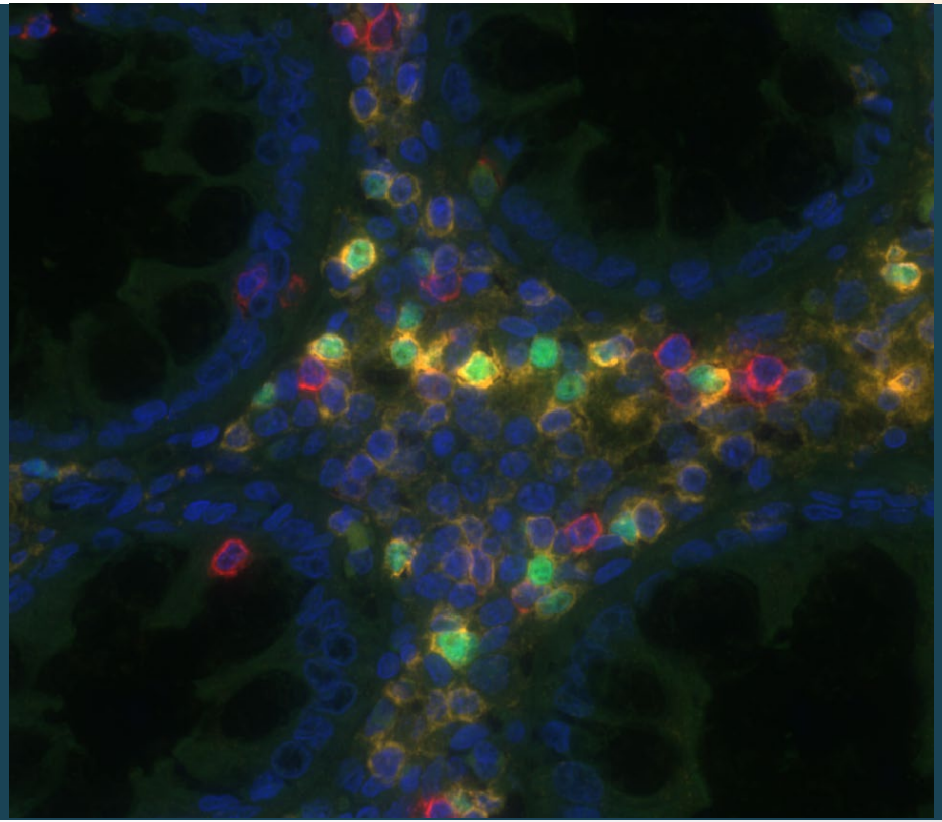

DAPI

CD4

CD8

Foxp3

Courtesy Dr. Melanie McCoy, University of Western Australia, Perth

APPLICATION NOTE:
PHENOTYPE OF TISSUE INFILTRATING LEUKOCYTES

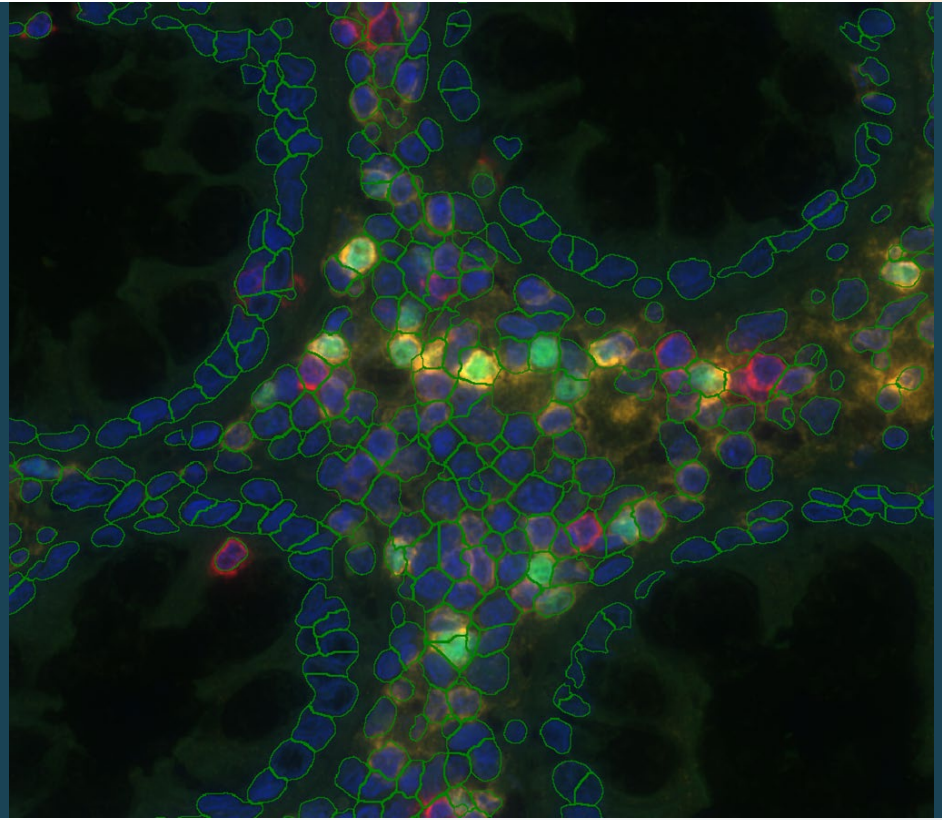

DAPI

CD4

CD8

Foxp3

Courtesy Dr. Melanie McCoy, University of Western Australia, Perth

APPLICATION NOTE:
PHENOTYPE OF TISSUE INFILTRATING LEUKOCYTES

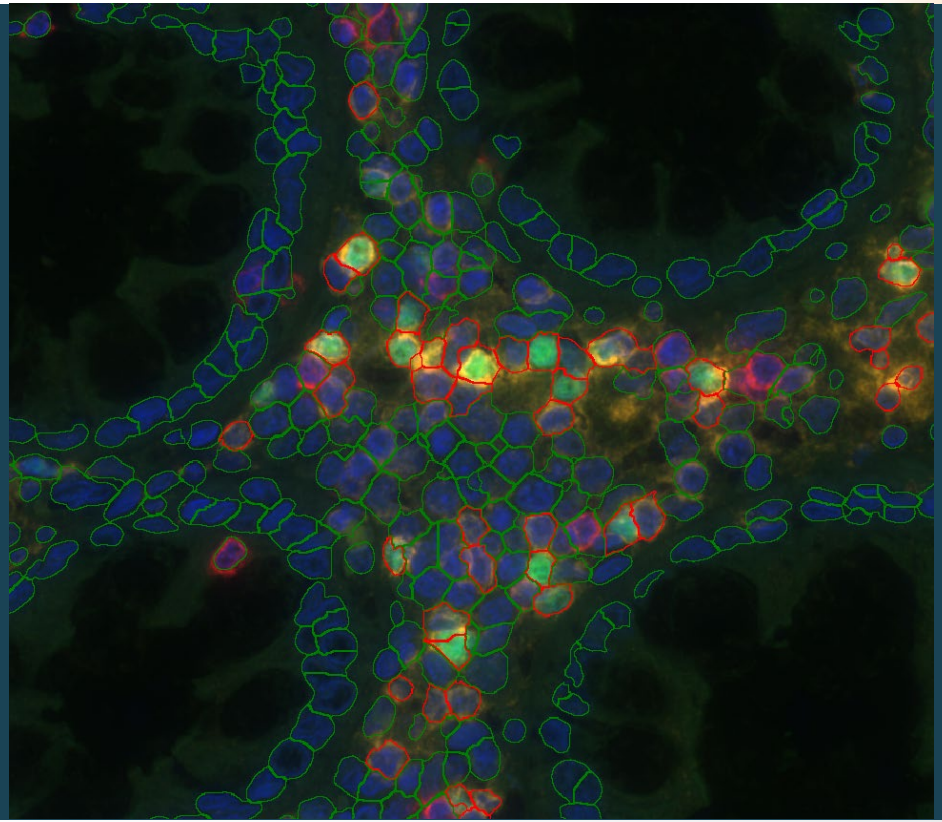

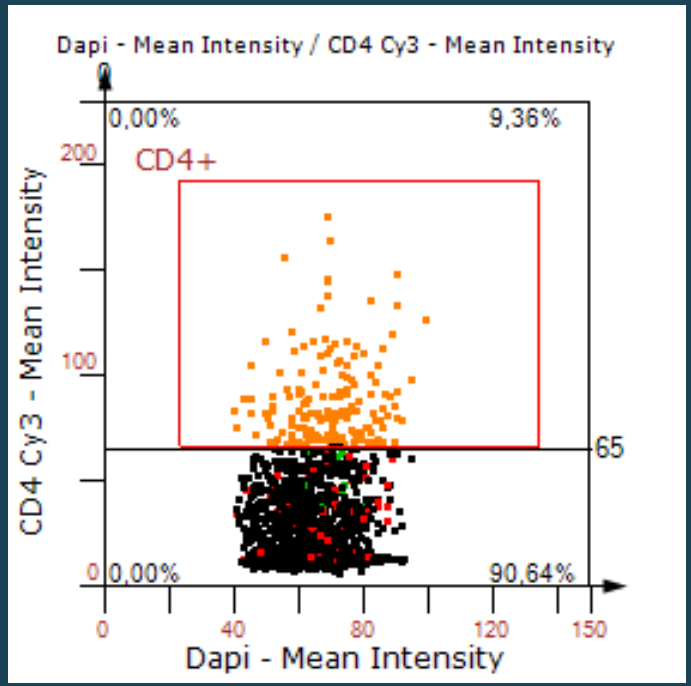

Courtesy Dr. Melanie McCoy, University of Western Australia, Perth

APPLICATION NOTE:
PHENOTYPE OF TISSUE INFILTRATING LEUKOCYTES

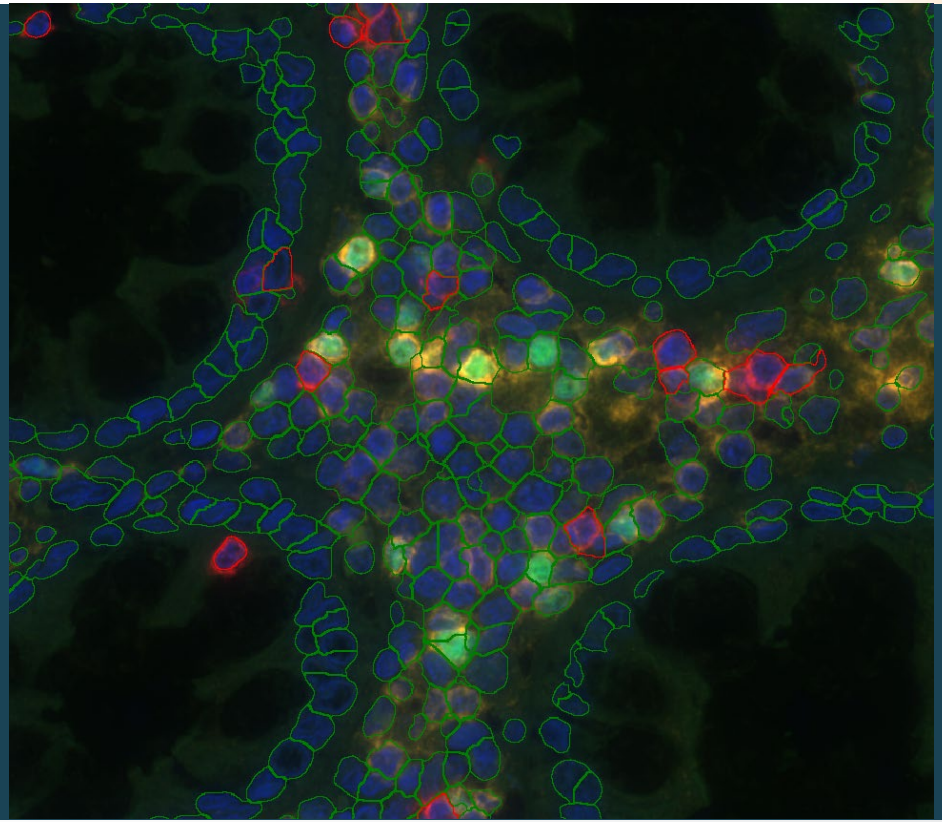

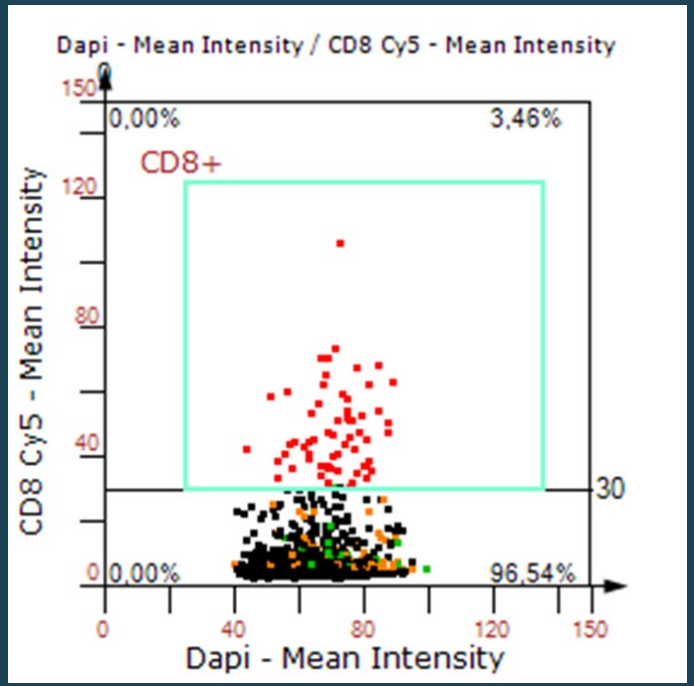

Courtesy Dr. Melanie McCoy, University of Western Australia, Perth

APPLICATION NOTE:
PHENOTYPE OF TISSUE INFILTRATING LEUKOCYTES

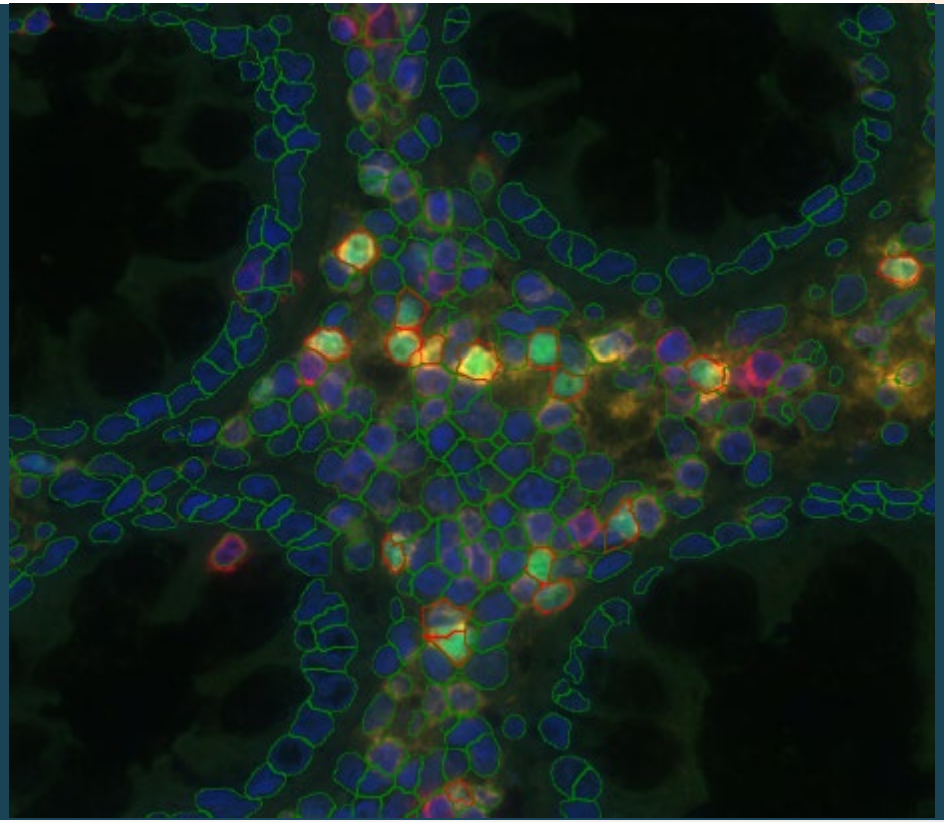

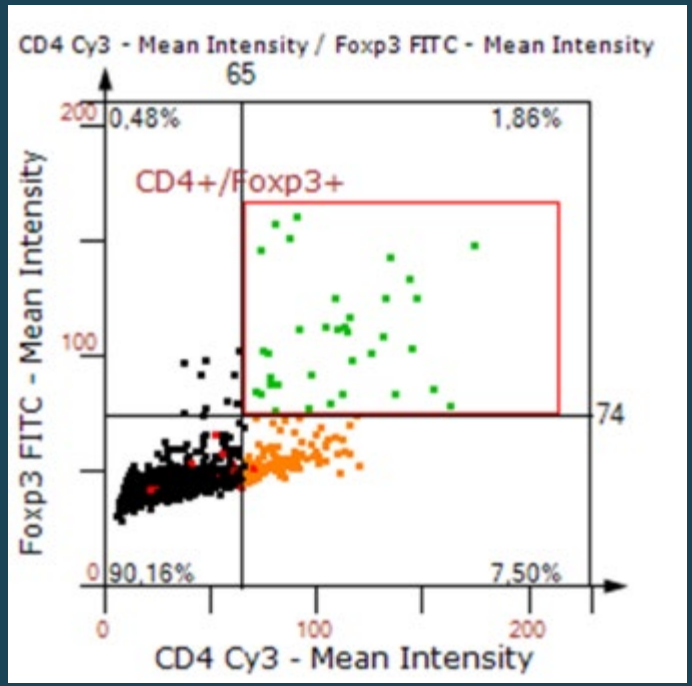

Courtesy Dr. Melanie McCoy, University of Western Australia, Perth

QUANTIFICATION OF CELLULAR COMPARTMENTS

INTRACELLULAR PARASITES

PLOS ONE

RESEARCH ARTICLE

An Emerging Approach for Parallel Quantification of Intracellular Protozoan Parasites and Host Cell Characterization Using TissueFAXS Cytometry

Maximilian Schmid[1], Bianca Dufner[1], Julius Dürk[1], Konstanze Bedal[1], Kristina Stricker[1], Lukas Ali Prokoph[1], Christoph Koch[1], Anja K. Wege[2], Henner Zirpel[3], Ger van Zandbergen[2,4], Rupert Ecker[5], Bogdan Boghiu[5], Uwe Ritter[1]*

1 Institute of Immunology, University of Regensburg, Regensburg, Germany, **2** Department of Gynecology and Obstetrics, University of Regensburg, Regensburg, Germany, **3** Division of Immunology, Paul-Ehrlich-Institute, Langen, Germany, **4** Institute of Immunology, University Medical Center of the Johannes Gutenberg University of Mainz, Mainz, Germany, **5** TissueGnostics GmbH, Vienna, Austria

Abstract

Characterization of host-pathogen interactions is a fundamental approach in microbiological and immunological oriented disciplines. It is commonly accepted that host cells start to change their phenotype after engulfing pathogens. Techniques such as real time PCR or ELISA were used to characterize the genes encoding proteins that are associated either with pathogen elimination or immune escape mechanisms. Most of such studies were performed *in vitro* using primary host cells or cell lines. Consequently, the data generated with such approaches reflect the global RNA expression or protein amount recovered from all cells in

Courtesy Prof. Uwe Ritter, Institute for Immunology, University of Regensburg, Germany

INTRACELLULAR PARASITES

Leishmaniasis:

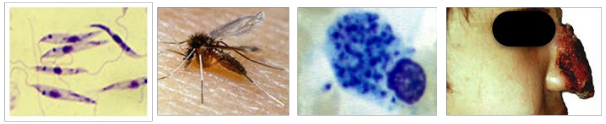

Experimental leishmaniasis:

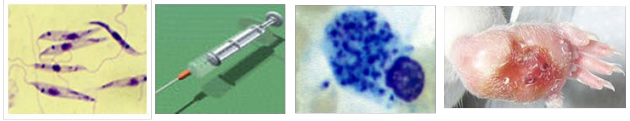

Host parasite interactions -> immune escape
Adaptive immunity -> parasite elimination

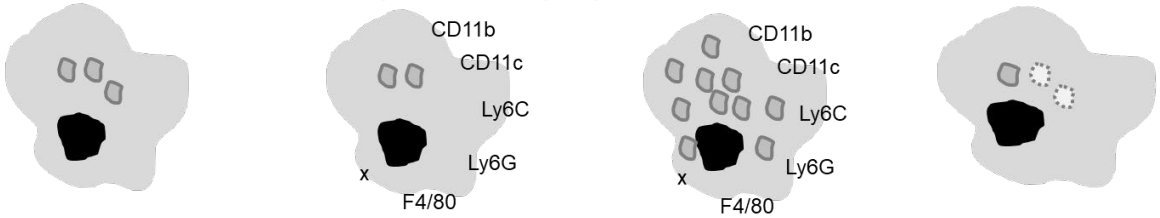

What is the parasite load?

Which cells control parasite replication?

Which cells are save host cells for parasites?

Which compounds induce leishmanicidal mechanisms?

System requirements:

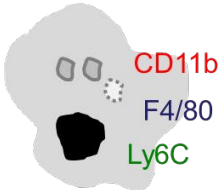

- Host cell detection
- Parasite detection (alive or dead)
- Mean fluorescence intensity analysis of markers

Ritter U. Book chapter, Protozoa, Immune Response to Parasitic Infections Vol-1. Bentham-Press. 2010

INTRACELLULAR PARASITES

Infection DAPI labelling → Gray scale image acquisition

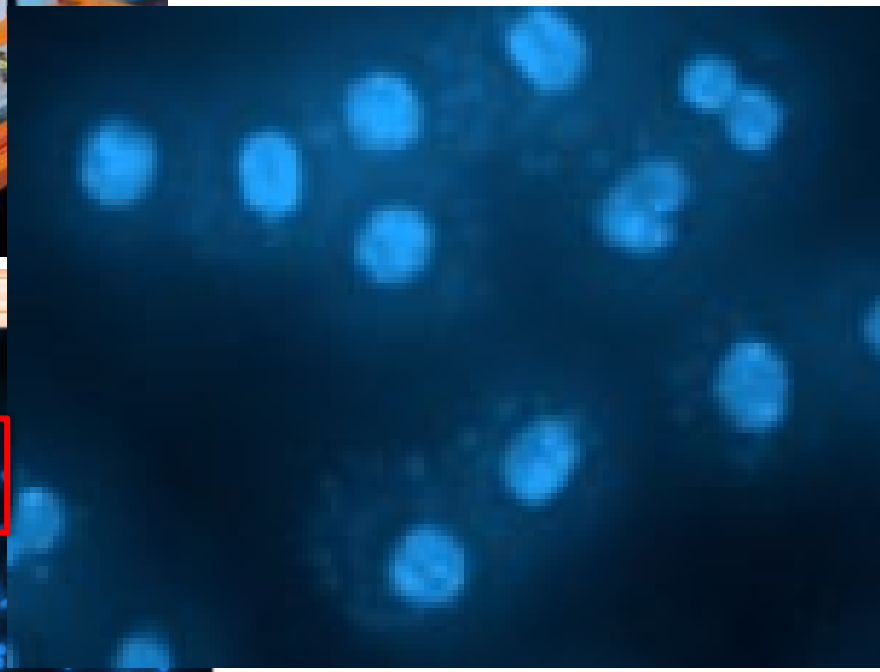

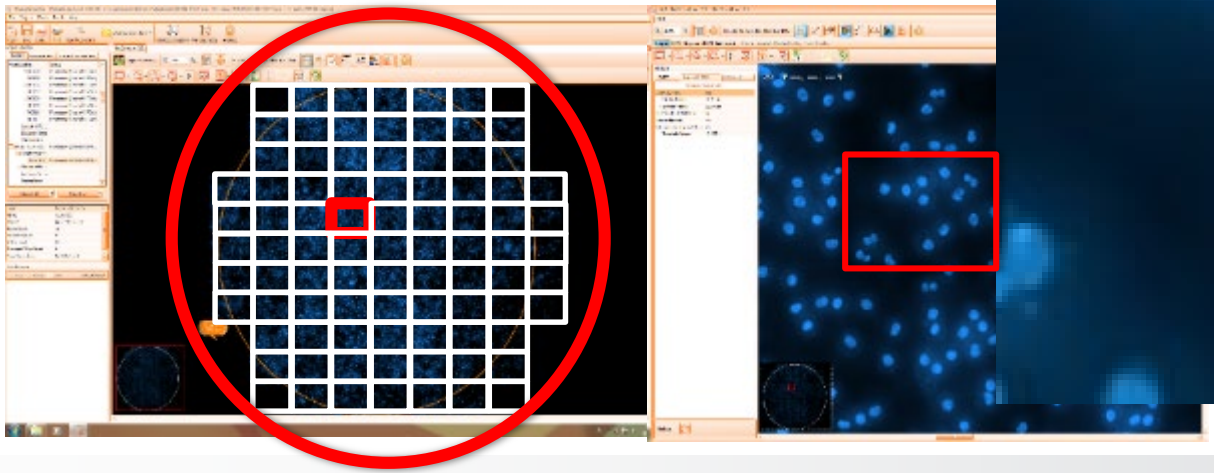

Courtesy Prof. Uwe Ritter, Institute for Immunology, University of Regensburg, Germany

INTRACELLULAR PARASITES

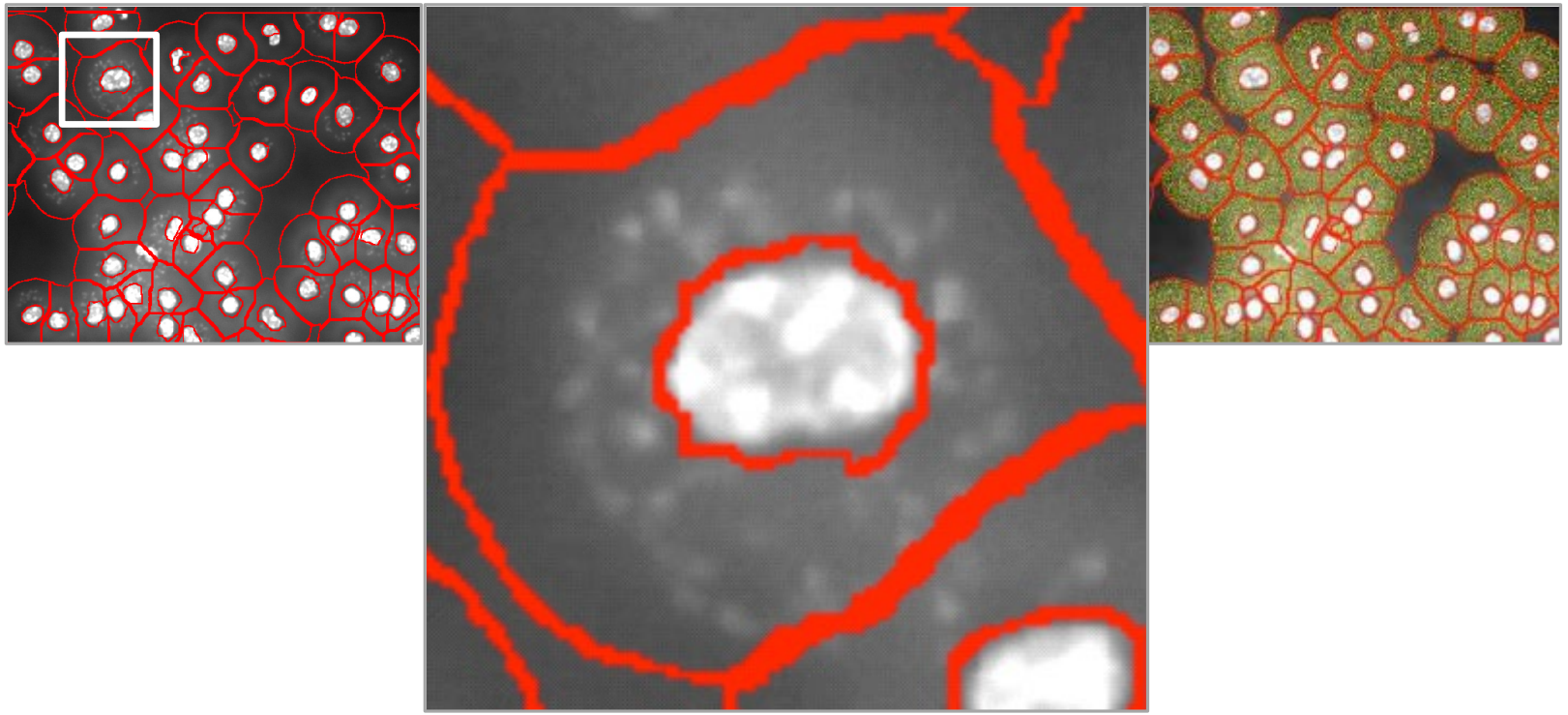

Red line: detection of nuclei and cell boarders
Yellow dotted area: cytoplasm

Courtesy Prof. Uwe Ritter, Institute for Immunology, University of Regensburg, Germany

INTRACELLULAR PARASITES

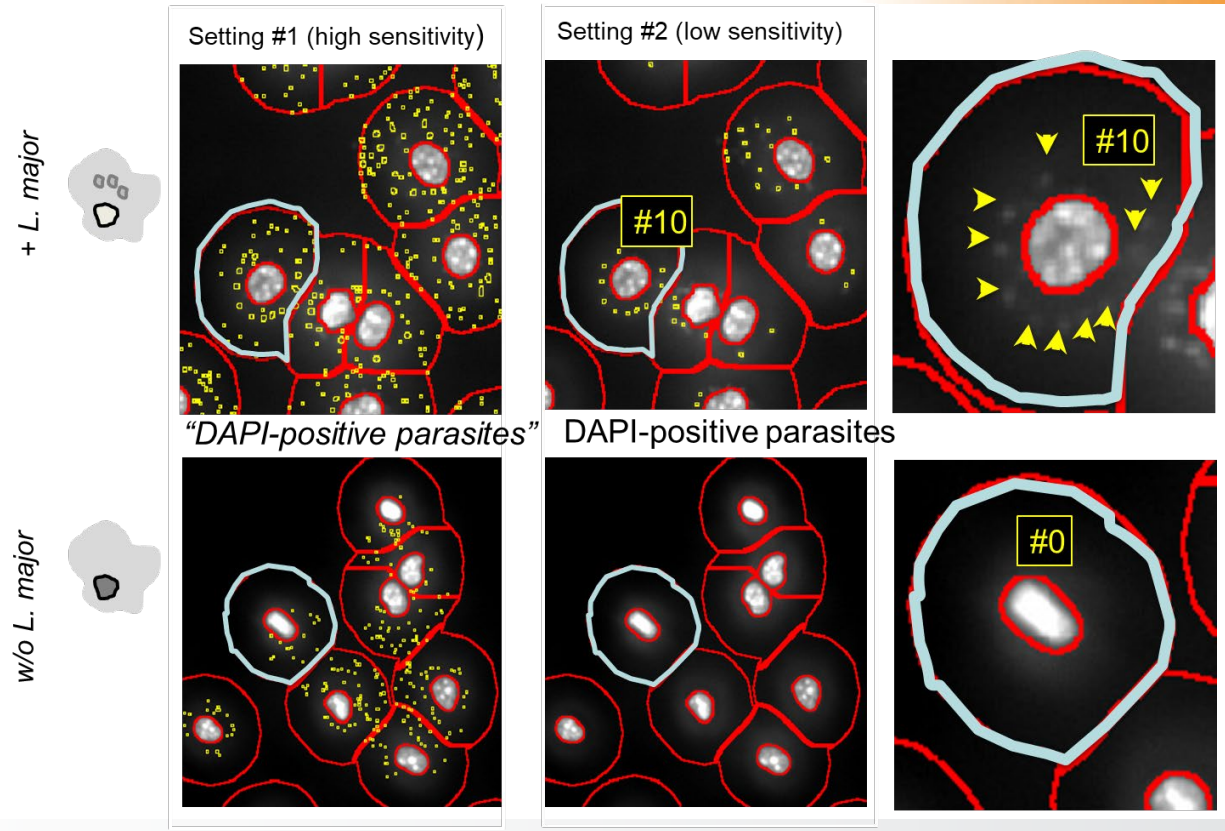

Courtesy Prof. Uwe Ritter, Institute for Immunology, University of Regensburg, Germany

INTRACELLULAR PARASITES

Can macrophages kill the parasites?

- Infection of macrophages (72h)
- Stimulation with IFN-gamma
- Ethidium bromide (EB)/ Acredine orange (AO) staining
- Fixation with PFA
- Parallel detection of EB+ and AO+ parasites

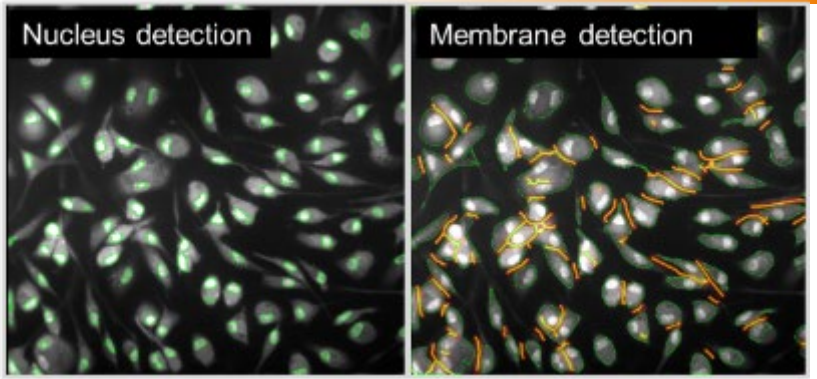

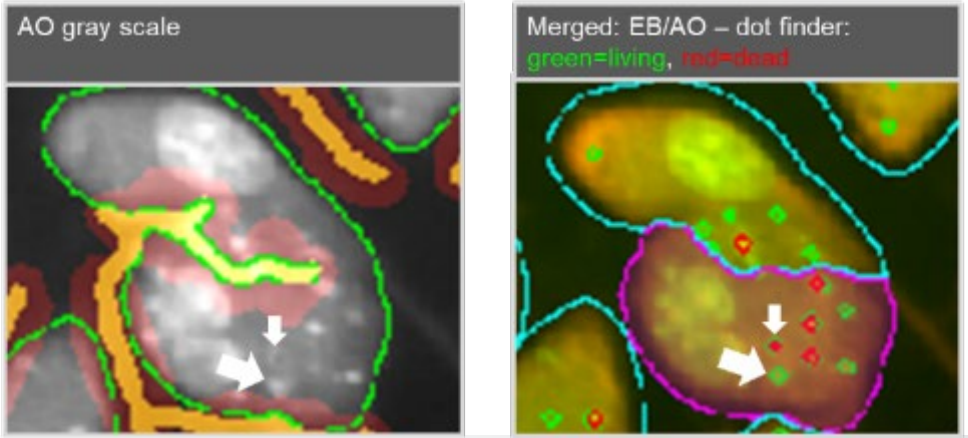

Courtesy Prof. Uwe Ritter, Institute for Immunology, University of Regensburg, Germany

MOLECULAR MECHANISMS OF INFLUENZA INFECTION AND PNEUMONIA

OX40 ligand newly expressed on bronchiolar progenitors mediates influenza infection and further exacerbates pneumonia

EMBO Molecular Medicine

Impact Factor 2019: 10.6

Taizou Hirano[1], Toshiaki Kikuchi[1,*,†], Naoki Tode[1], Arif Santoso[1], Mitsuhiro Yamada[1], Yoshiya Mitsuhashi[1], Riyo Komatsu[1], Takeshi Kawabe[2], Takeshi Tanimoto[3], Naoto Ishii[2], Yuetsu Tanaka[4], Hidekazu Nishimura[5], Toshihiro Nukiwa[1], Akira Watanabe[6] & Masakazu Ichinose[1]

1 Department of Respiratory Medicine, Tohoku University Graduate School of Medicine, Sendai, Japan
2 Department of Microbiology and Immunology, Tohoku University Graduate School of Medicine, Sendai, Japan
3 Kanonji Institute, The Research Foundation for Microbial Diseases of Osaka University, Kanonji, Japan
4 Department of Immunology, Graduate School of Medicine, University of the Ryukyus, Okinawa, Japan
5 Virus Research Center, Sendai Medical Center, National Hospital Organization, Sendai, Japan
6 Research Division for Development of Anti-Infective Agents, Institute of Development, Aging and Cancer, Tohoku University, Sendai, Japan
*Corresponding author. Tel: +81 25 368 9321; Fax: +81 25 368 9326; E-mail: kikuchi@med.niigata-u.ac.jp
†Present address: Department of Respiratory Medicine and Infectious Diseases, Niigata University Graduate School of Medical and Dental Sciences, Niigata, Japan

TISSUEFAXS™ CYTOMETRY: INFLUENZA & PNEUMONIA

Abstract

Influenza virus epidemics potentially cause pneumonia, which is responsible for much of the mortality due to the excessive immune responses. The role of costimulatory OX40–OX40 ligand (OX40L) interactions has been explored in the non-infectious pathology of influenza pneumonia. Here, we describe a critical contribution of OX40L to infectious pathology, with OX40L deficiency, but not OX40 deficiency, resulting in decreased susceptibility to influenza viral infection. Upon infection, bronchiolar progenitors increase in number for repairing the influenza-damaged epithelia. The OX40L expression is induced on the progenitors for the antiviral immunity during the infectious process. However, these defense-like host responses lead to more extensive infection owing to the induced OX40L with α-2,6 sialic acid modification, which augments the interaction with the viral hemagglutinin. In fact, the specific antibody against the sialylated site of OX40L exhibited therapeutic potency in mitigating the OX40L-mediated susceptibility to influenza. Our data illustrate that the influenza-induced expression of OX40L on bronchiolar progenitors has pathogenic value to develop a novel therapeutic approach against influenza.

EMBO Molecular Medicine

Impact Factor 2019: 10.6

Keywords bronchioles; glycosylation regeneration; OX40 ligand; viral pneumonia

TISSUEFAXS™ CYTOMETRY: INFLUENZA & PNEUMONIA

Immunofluorescence

For immunocytochemistry, 2 × 10^4 cells were cytospun onto glass slides (600 × *g*, 2 min) and were fixed in 10% neutral buffered formalin for 20 min. After being treated with Protein Block Serum-Free (Dako, Carpinteria, CA) for 30 min, the cytospun cells were incubated with primary monoclonal antibodies to influenza A virus M2 protein (clone 14C2, 1:500, Abcam) and to mouse OX40L (clone RM134L, 1:500, eBioscience) for overnight at 4°C. For immunofluorescent staining of lung tissues, 5-µm cryosections were dehydrated in 100% ethanol and rehydrated in decreasing concentrations of ethanol in PBS. When necessary, antigen retrieval was performed by incubation in water-diluted Histofine (pH 9, Nichirei) and treatment with an autoclave (15 min, 121°C). After the Protein Block Serum-Free treatment, the following primary antibodies were added and incubated for overnight at 4°C: anti-CCSP (club cell secretory protein, 1:500, Santa Cruz Biotechnology, Dallas, TX) and anti-SPC (surfactant protein C, 1:500, Santa Cruz Biotechnology), or anti-influenza A virus M2 protein (clone 14C2, 1:500, Abcam). Slides were treated with a fluorescence-labeled secondary antibody (1:200, Life Technologies) for 1 h at 25°C and were mounted using VECTASHIELD Mounting Medium with DAPI (4′,6-diamidino-2-phenylindole, Vector Laboratories, Burlingame, CA). Fluorescent images were acquired by using an LSM 780 confocal microscope (Carl Zeiss, Oberkochen, Germany) and were analyzed by 2 independent investigators (Kikuchi and Tode). Where indicated, the images were quantified by using a TissueFAXS system (TissueGnostics, Vienna, Austria).

EMBO Molecular Medicine

Impact Factor 2019: 10.6

TISSUEFAXS™ CYTOMETRY: INFLUENZA & PNEUMONIA

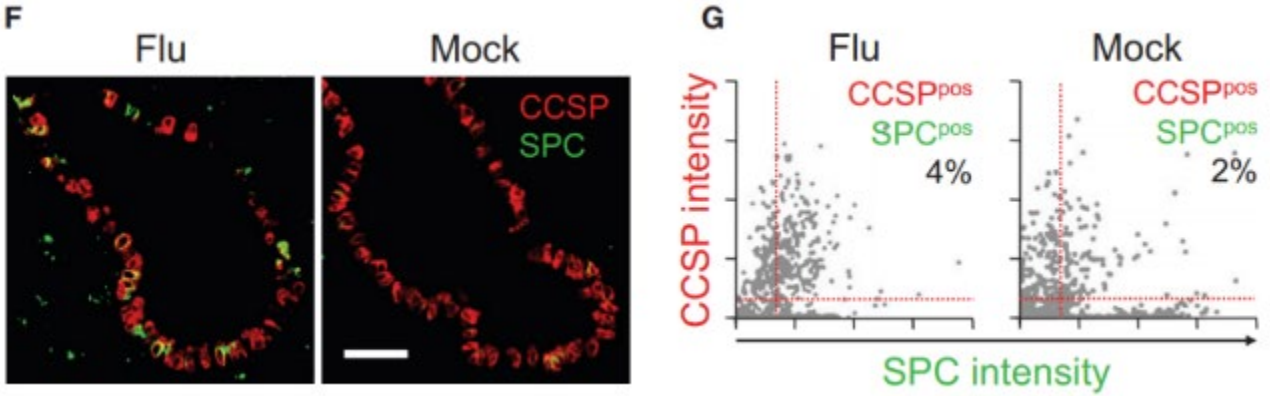

Figure 2. Both the number and the OX40L expression level of bronchiolar progenitors were increased by influenza infection.

Wild-type mice were intratracheally infected with a lethal dose of influenza A/H1N1 virus (Flu) or saline (Mock), and 7 days later, their lung cells and sections were evaluated.

- A Cell counts of OX40L-positive cells in whole lung cells.
- B Status of CD31 and CD45 expression in lung OX40L-positive cells.
- C Status of Sca-1 expression and autofluorescence in lung OX40L-positive Lin-negative (i.e., $OX40L^{pos}CD31^{neg}CD45^{neg}CD34^{neg}$) cells.
- D, E (D) Proportion of bronchiolar progenitors ($Lin^{neg}Sca\text{-}1^{low}AF^{low}$, red box) and club cells ($Lin^{neg}Sca\text{-}1^{low}AF^{high}$, blue box), and (E) their cell counts.
- F, G (F) Lung sections stained with antibodies to CCSP (red) and SPC (green), and (G) quantitative analysis of these imaging data. Scale bar, 50 μm.
- H Cell counts of OX40L-positive cells in bronchiolar progenitors and club cells.
- I *OX40L* gene expression in bronchiolar progenitors and club cells. By quantitative RT–PCR, the gene expression levels were analyzed relative to the bronchiolar progenitors of mock-infected mice. ND, not determined for scarcity of club cells after influenza infection.

Data information: Data are presented as the mean ± standard error of $n = 4$ (A and E) or $n = 3$ (I) per group. Student's unpaired two-tailed t-test (A and I): $P = 0.0001$ (A): progenitors, $P = 0.0102$ (I). Tukey's honestly significant difference test (E): progenitors, $P = 0.0001$; club cells, $P = 0.0097$.

Source data are available online for this figure.

EMBO Molecular Medicine

Impact Factor 2019: 10.6

MOLECULAR MECHANISMS OF ZIKA VIRUS INFECTION

TISSUEFAXS™ CYTOMETRY: ZIKA VIRUS INFECTION

nature microbiology

Letter | Published: 29 January 2018

Impact Factor 2019: 14.3

AXL promotes Zika virus infection in astrocytes by antagonizing type I interferon signalling

Jian Chen, Yi-feng Yang, Yu Yang, Peng Zou, Jun Chen, Yongquan He, Sai-lan Shui, Yan-ru Cui, Ru Bai, Ya-jun Liang, Yunwen Hu, Biao Jiang, Lu Lu, Xiaoyan Zhang ✉, Jia Liu ✉ & Jianqing Xu ✉

Nature Microbiology **3**, 302–309(2018) | Cite this article

1248 Accesses | **36** Citations | **17** Altmetric | Metrics

[1]Scientific Research Center, Shanghai Public Health Clinical Center & Institutes of Biomedical Sciences, Key Laboratory of Medical Molecular Virology of Ministry of Education/Health, Shanghai Medical College, Fudan University, Shanghai, China. [2]Shanghai Institute for Advanced Immunochemical Studies, ShanghaiTech University, Shanghai, China. [3]Department of Ecology and Genetics, Evolutionary Biology Centre, Uppsala University, Uppsala, Sweden. [4]State Key Laboratory for Infectious Disease Prevention and Control, China Centers for Disease Control and Prevention, Beijing, China. Jian Chen and Yi-feng Yang contributed equally to this work. Deceased: Yunwen Hu. *e-mail: zhangxiaoyan@shaphc.org.cn; liujia@shanghaitech.edu.cn; xujianqing@shaphc.org.cn

Abstract

Zika virus (ZIKV) is associated with neonatal microcephaly and Guillain–Barré syndrome[1,2]. While progress has been made in understanding the causal link between ZIKV infection and microcephaly[3,4,5,6,7,8,9], the life cycle and pathogenesis of ZIKV are less well understood. In particular, there are conflicting reports on the role of AXL, a TAM family kinase receptor that was initially described as the entry receptor for ZIKV[10,11,12,13,14,15,16,17,18,19,20,21,22]. Here, we show that while genetic ablation of AXL protected primary human astrocytes and astrocytoma cell lines from ZIKV infection, AXL knockout did not block the entry of ZIKV. We found, instead, that the presence of AXL attenuated the ZIKV-induced activation of type I interferon (IFN) signalling genes, including several type I IFNs and IFN-stimulating genes. Knocking out type I IFN receptor α chain (IFNAR1) restored the vulnerability of AXL knockout astrocytes to ZIKV infection. Further experiments suggested that AXL regulates the expression of SOCS1, a known type I IFN signalling suppressor, in a STAT1/STAT2-dependent manner. Collectively, our results demonstrate that AXL is unlikely to function as an entry receptor for ZIKV and may instead promote ZIKV infection in human astrocytes by antagonizing type I IFN signalling.

TISSUEFAXS™ CYTOMETRY: ZIKA VIRUS INFECTION

Immunofluorescence and in situ hybridization (ISH)

Immunofluorescence analyses of ZIKV infection were performed using mouse anti-flavivirus envelope protein antibodies (1:200, clone D1-4G2-4-15, Millipore) and Alexa Fluor 568 donkey anti-mouse IgG (H + L) (1:1,000, ab175472, Abcam). To detect GFAP, astrocytes were incubated with rabbit anti-GFAP antibodies (1:200, ab68428, Abcam) and Alexa Fluor 488 donkey anti-rabbit IgG (H + L) (1:1,000, ab150077, Abcam). ISH was performed using an RNAscope Fluorescent Multiplex Assay kit (Advanced Cell Diagnostics) according to the manufacturer's instructions. NBF-fixed tissue slides were hydrated and then successively immersed in 200 ml of 50% ethanol, 200 ml of 70% ethanol and 400 ml of 100% ethanol for 5 minutes each at room temperature. ZIKV genomic RNA was detected using a premade RNA probe (red fluorescence) obtained from Advanced Cell Diagnostics (Cat No. 467771). Immunofluorescence and ISH images were acquired and analysed using a TissueFAXS 200 flow-type tissue quantitative analyser (TissueGnostics GmbH, Vienna, Austria). All statistical results from immunofluorescence staining represent analyses of at least 10,000 cells in each replicate and are shown as the mean + s.d.

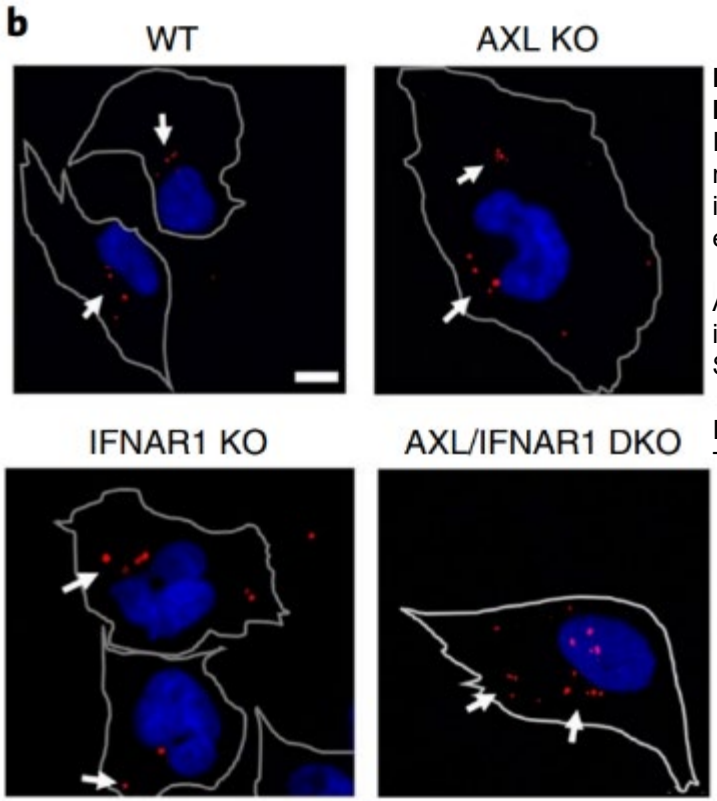

Detection of ZIKV RNA by ISH.
Images shown are representative of three independent experiments.

Arrows indicate internalized ZIKV RNA. Scale bar: 2.5 µm

Images acquired with TissueFAXS Cytometer

MOLECULAR MECHANISMS OF DENGUE VIRUS INFECTION

TISSUEFAXS™ CYTOMETRY: DENGUE VIRUS INFECTION

Therapeutic Effects of Monoclonal Antibody against Dengue Virus NS1 in a STAT1 Knockout Mouse Model of Dengue Infection

Shu-Wen Wan,[*,†,‡,1] Pei-Wei Chen,[†,1] Chin-Yu Chen,[†] Yen-Chung Lai,[§,¶] Ya-Ting Chu,[†] Chia-Yi Hung,[†] Han Lee,[†] Hsuan Franziska Wu,[‖] Yung-Chun Chuang,[¶] Jessica Lin,[¶] Chih-Peng Chang,[*,†] Shuying Wang,[*,†] Ching-Chuan Liu,[*,#] Tzong-Shiann Ho,[*,#] Chiou-Feng Lin,[*,**] Chien-Kuo Lee,[††] Betty A. Wu-Hsieh,[††] Robert Anderson,[‡‡,§§,¶¶] Trai-Ming Yeh,[*,¶] and Yee-Shin Lin[*,†]

Dengue virus (DENV) is the causative agent of dengue fever, dengue hemorrhagic fever, and dengue shock syndrome and is endemic to tropical and subtropical regions of the world. Our previous studies showed the existence of epitopes in the C-terminal region of DENV nonstructural protein 1 (NS1) which are cross-reactive with host Ags and trigger anti–DENV NS1 Ab–mediated endothelial cell damage and platelet dysfunction. To circumvent these potentially harmful events, we replaced the C-terminal region of DENV NS1 with the corresponding region from Japanese encephalitis virus NS1 to create chimeric DJ NS1 protein. Passive immunization of DENV-infected mice with polyclonal anti–DJ NS1 Abs reduced viral Ag expression at skin inoculation sites and shortened DENV-induced prolonged bleeding time. We also investigated the therapeutic effects of anti-NS1 mAb. One mAb designated 2E8 does not recognize the C-terminal region of DENV NS1 in which host–cross-reactive epitopes reside. Moreover, mAb 2E8 recognizes NS1 of all four DENV serotypes. We also found that mAb 2E8 caused complement-mediated lysis in DENV-infected cells. In mouse model studies, treatment with mAb 2E8 shortened DENV-induced prolonged bleeding time and reduced viral Ag expression in the skin. Importantly, mAb 2E8 provided therapeutic effects against all four serotypes of DENV. We further found that mAb administration to mice as late as 1 d prior to severe bleeding still reduced prolonged bleeding time and hemorrhage. Therefore, administration with a single dose of mAb 2E8 can protect mice against DENV infection and pathological effects, suggesting that NS1-specific mAb may be a therapeutic option against dengue disease. *The Journal of Immunology*, 2017, 199: 2834–2844.

The Journal of Immunology

Impact Factor 2019: 4.7

TISSUEFAXS™ CYTOMETRY: DENGUE VIRUS INFECTION

AUTHOR INFORMATION

Shu-Wen Wan[*,†,‡,1], Pei-Wei Chen[*,1], Chin-Yu Chen[*], Yen-Chung Lai[§,¶], Ya-Ting Chu[†], Chia-Yi Hung[†], Han Lee[‖], Hsuan Franziska Wu[‖], Yung-Chun Chuang[#], Jessica Lin[#], Chih-Peng Chang[*,‖], Shuying Wang[*,†], Ching-Chuan Liu[*,††], Tzong-Shiann Ho[*,††], Chiou-Feng Lin[*,**], Chien-Kuo Lee[††], Betty A. Wu-Hsieh[††], Robert Anderson[‡‡,§§,¶¶], Trai-Ming Yeh[*,¶] and Yee-Shin Lin[*,‖]

[*]*Center of Infectious Disease and Signaling Research, College of Medicine, National Cheng Kung University, Tainan 701, Taiwan;*

[†]*Department of Microbiology and Immunology, College of Medicine, National Cheng Kung University, Tainan 701, Taiwan;*

[‡]*School of Medicine, College of Medicine, I-Shou University, Kaohsiung 824, Taiwan;*

[§]*Institute of Basic Medical Sciences, College of Medicine, National Cheng Kung University, Tainan 701, Taiwan;*

[¶]*Department of Medical Laboratory Science and Biotechnology, College of Medicine, National Cheng Kung University, Tainan 701, Taiwan;*

[‖]*Department of Medicine, College of Medicine, National Cheng Kung University, Tainan 701, Taiwan;*

[#]*Department of Pediatrics, College of Medicine, National Cheng Kung University, Tainan 701, Taiwan;*

[**]*Department of Microbiology and Immunology, College of Medicine, Taipei Medical University, Taipei 110, Taiwan;*

[††]*Graduate Institute of Immunology, National Taiwan University College of Medicine, Taipei 100, Taiwan;*

[‡‡]*Department of Microbiology and Immunology, Dalhousie University, Halifax, Nova Scotia B3H 4R2, Canada;*

[§§]*Department of Pediatrics, Dalhousie University, Halifax, Nova Scotia B3H 4R2, Canada; and*

[¶¶]*Canadian Center for Vaccinology, Dalhousie University, Halifax, Nova Scotia B3H 4R2, Canada*

Immunohistochemistry staining

The skin sections were embedded in paraffin and sliced on slides. Slides were deparaffinized using xylene and graded alcohol (100, 95, 85, 70, and 50%). The sections were then incubated in 2 N HCl solution for 20 min followed by treatment with 20 μg/ml proteinase K in TE buffer (50 mM Tris Base, 1 mM EDTA, and 0.5% Triton X-100, pH 8) for another 20 min at room temperature. The sections were then incubated with 3% H_2O_2 in PBS for 15 min, to inhibit endogenous peroxidase activity, and blocked with 5% BSA in PBS with Tween 20 (PBS-T). The primary and secondary Abs were adequately diluted in Ab diluents (Dako, Carpentaria, CA). The DENV Ag was stained with polyclonal anti–DENV NS3 Abs (GeneTex, Irvine, CA) overnight at 4°C, followed by biotin-labeled donkey anti-rabbit Abs at room temperature for 1 h. The skin sections were developed with the AEC substrate kit (Dako) and nuclei were further stained with hematoxylin for 10 s. The sections were also analyzed using a TissueFAXS (TissueGnostics, Vienna, Austria) image cytometer and quantified with the HistoQuest software (TissueGnostics) using an average of 15 fields of view. This procedure was followed as previously reported (14).

TISSUEFAXS™ CYTOMETRY: DENGUE VIRUS INFECTION

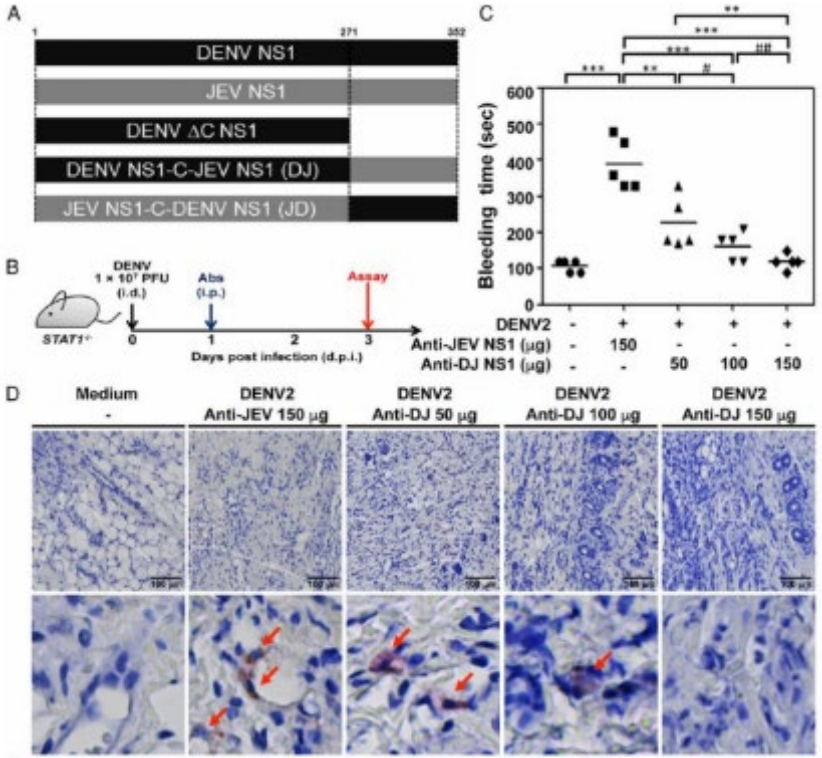

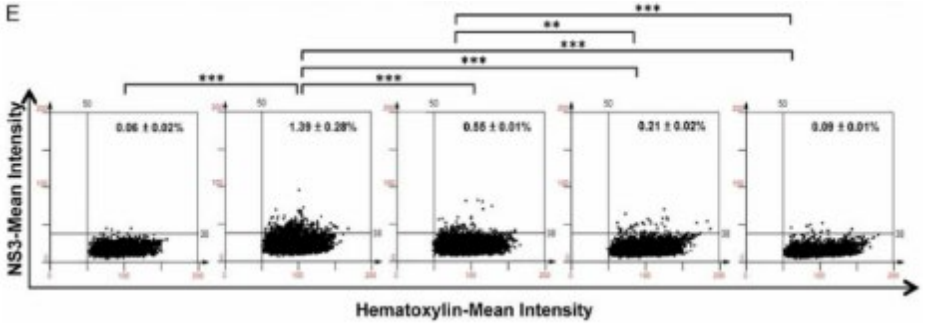

Passive immunization with a single dose of anti–DJ NS1 Abs can shorten DENV-induced bleeding tendency and reduce DENV NS3 expression in DENV-infected *STAT1*$^{-/-}$ mice. (**A**) The C-terminal region of DENV NS1 protein from amino acids 271–352 was deleted to generate ΔC NS1 protein or replaced with C-terminal JEV NS1 (amino acids 271–352) to generate DJ NS1 protein. (**B**) Experimental design of the DENV-infected therapeutic model in *STAT1*$^{-/-}$ mice. (**C**) Mice were i.d. inoculated with 1 ×10^7 PFU per mouse of DENV2 and i.p. injected with anti–JEV NS1 Abs or anti–DJ NS1 Abs at 1 d.p.i. (n = 5 mice per group). The mouse-tail bleeding time was determined at 3 d.p.i. (**D**) The local skin injection site sections of *STAT1*$^{-/-}$ mice were stained with anti–DENV NS3 Abs (red), and nuclei were stained with hematoxylin (blue). The lower panels show enlarged images of the boxed areas in the upper panels. Red arrows indicate the NS3-positive cells (original magnification ×200; scale bars, 100 μm). (**E**) The NS3-positive cells were counted in 15 regions per mouse skin section and the average numbers of positively stained cells were calculated by HistoQuest software. The scattergram plots of each group are shown and the percentages of NS3-positive cells are shown as mean ± SD. $^{**}p < 0.01$, $^{***}p < 0.001$, $^{\#}p - 0.08$, $^{\#\#}p - 0.64$, one-way ANOVA with Tukey post hoc test.

MULTISPECTRAL IMAGING & SPECTRAL UNMIXING

SPECTRAL IMAGING

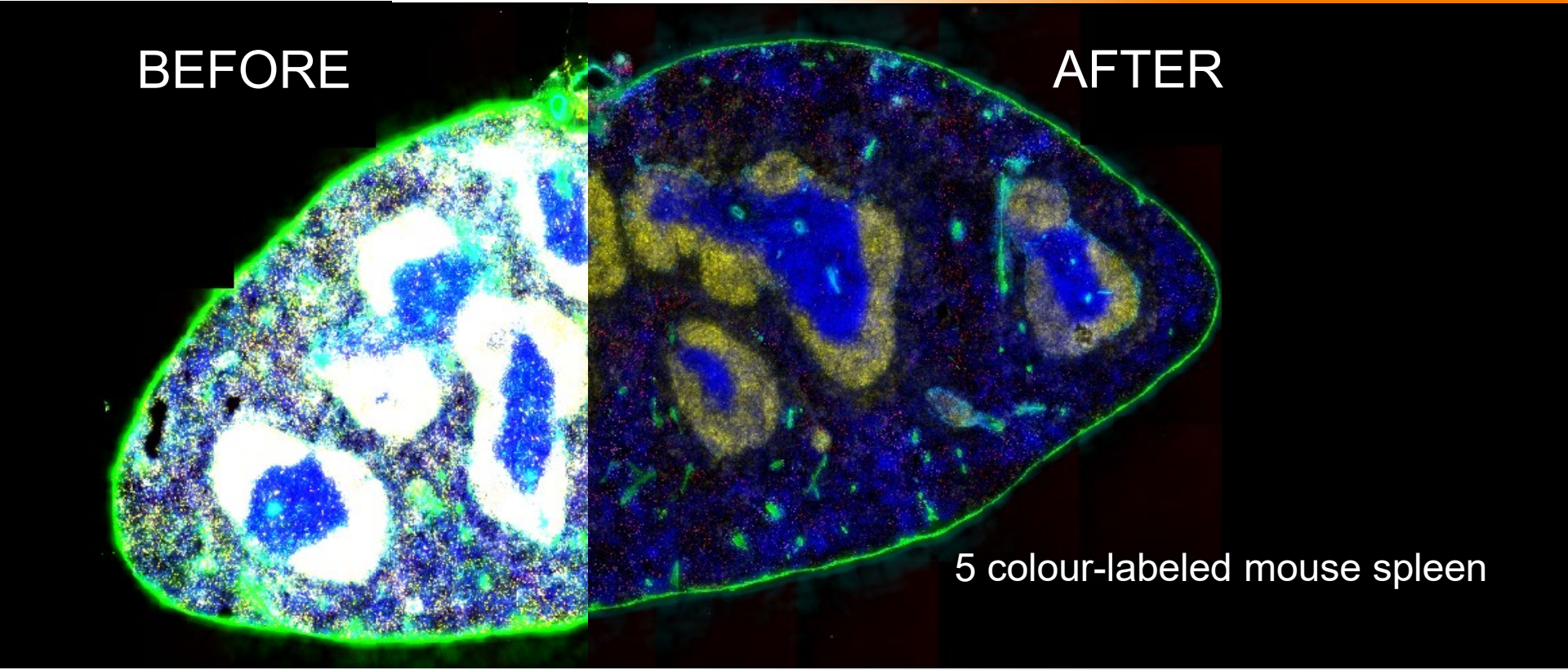

Courtesy Dr. Ulf Yrlid, University of Gothenburg, Sweden, EU

SPECTRAL IMAGING OF COVID-19 TISSUE

Cell

CellPress

Article

Loss of Bcl-6-Expressing T Follicular Helper Cells and Germinal Centers in COVID-19

Naoki Kaneko,[1,8] Hsiao-Hsuan Kuo,[1,8] Julie Boucau,[1,8] Jocelyn R. Farmer,[1,8] Hugues Allard-Chamard,[1,4] Vinay S. Mahajan,[1,2] Alicja Piechocka-Trocha,[1,6] Kristina Lefteri,[1] Matthew Osborn,[1] Julia Bals,[1] Yannic C. Bartsch,[1] Nathalie Bonheur,[1] Timothy M. Caradonna,[1] Josh Chevalier,[1] Fatema Chowdhury,[1] Thomas J. Diefenbach,[1] Kevin Einkauf,[1] Jon Fallon,[1] Jared Feldman,[1] Kelsey K. Finn,[1] Pilar Garcia-Broncano,[1] Ciputra Adijaya Hartana,[1] Blake M. Hauser,[1] Chenyang Jiang,[1] Paulina Kaplonek,[1] Marshall Karpell,[1] Eric C. Koscher,[1] Xiaodong Lian,[1] Hang Liu,[1] Jinqing Liu,[1] Ngoc L. Ly,[1] Ashlin R. Michell,[1] Yelizaveta Rassadkina,[1] Kyra Seiger,[1] Libera Sessa,[1] Sally Shin,[1] Nishant Singh,[1] Weiwei Sun,[1] Xiaoming Sun,[1] Hannah J. Ticheli,[1] Michael T. Waring,[1,6] Alex L. Zhu,[1] Galit Alter,[1] Jonathan Z. Li,[3] Daniel Lingwood,[1] Aaron G. Schmidt,[1,5] Mathias Lichterfeld,[1,3] Bruce D. Walker,[1,6,7] Xu G. Yu,[1,3] Robert F. Padera, Jr.,[2,*] Shiv Pillai,[1,9,*] and the Massachusetts Consortium on Pathogen Readiness Specimen Working Group

[1]Ragon Institute of MGH, MIT and Harvard, Cambridge, MA 02139, USA
[2]Department of Pathology, Brigham and Women's Hospital, Boston, MA 02115, USA
[3]Department of Medicine, Brigham and Women's Hospital, Boston, MA 02115, USA
[4]Division of Rheumatology, Faculté de Médecine et des Sciences de la Santé de l'Université de Sherbrooke et Centre de Recherche Clinique Étienne-Le Bel, Sherbrooke, QC J1K 2R1, Canada
[5]Department of Microbiology, Harvard Medical School, Boston, MA 02115, USA
[6]Howard Hughes Medical Institute, Chevy Chase, MD 20815, USA
[7]Department of Biology and Institute of Medical Engineering and Science, Massachusetts Institute of Technology, Cambridge, MA 02139, USA
[8]These authors contributed equally
[9]Lead Contact
*Correspondence: rpadera@bwh.harvard.edu (R.F.P.), pillai@helix.mgh.harvard.edu (S.P.)

Quantification of the immune response against SARS-CoV-2 by multi-spectral tissue cytometry

Published online: 25.08.2020

Printed: 01.10.2020

Impact Factor: 38.6

SPECTRAL IMAGING OF COVID-19 TISSUE

Multi-color immunofluorescence staining

Tissue samples were fixed in formalin, embedded in paraffin, and sectioned. These specimens were incubated with the following antibodies: anti-CD3 (clone: A045229-2; DAKO), anti-CD4 (clone: EPR6855;Abcam), anti-CD19 (clone: SKU310; Biocare Medical), anti-Bcl6 (clone: LN22; Biocare Medical), anti-AID (clone: ZA001; Invitrogen), anti-T-bet (clone: ab150440; Abcam), GATA3 (clone: CM405A; Biocare), ICOS (clone: 89601; Cell Signaling Technology), Rorc (clone: ab212496; Abcam), CXCR5 (clone: MAB190; R&D Systems), Foxp3 (clone: 98377; Cell Signaling Technology), anti-CD8 (clone: ab85792; Abcam), anti-IgD (clone: AA093; DAKO), anti-CD27 (clone: ab131254; Abcam), anti-IgG (clone: ab109489; Abcam), anti-TNF-α (clone: ab6671; Abcam), and anti-CD35 (clone: ab25; Abcam) followed by incubation with a secondary antibody using an Opal Multiplex Kit (Perkin Elmer). The samples were mounted with ProLong Diamond Antifade mountant containing DAPI (Invitrogen).

Microscopy and Quantitative Image Analysis

Images of the tissue specimens were acquired using the TissueFAXS platform (TissueGnostics). For quantitative analysis, the entire area of the tissue was acquired as a digital grayscale image in five channels with filter settings for FITC, Cy3, Cy5 and AF75 in addition to DAPI. Cells of a given phenotype were identified and quantitated using the TissueQuest software (TissueGnostics), with cut-off values determined relative to the positive controls. This microscopy-based multicolor tissue cytometry software permits multicolor analysis of single cells within tissue sections similar to flow cytometry. In addition, multispectral images (seven-colors staining) were unmixed using spectral libraries built from images of single stained tissues for each reagent using the StrataQuest (TissueGnostics) software. StrataQuest software was also used to quantify cell-to-cell contact. In the StrataQuest cell-to-cell contact application, masks of the nuclei based on DAPI staining establish the inner boundary of the cytoplasm and the software "looks" outward toward the plasma membrane boundary. Overlap of at least 3 pixels of adjacent cell markers is required to establish a "contact" criterion. Although the software has been developed and validated more recently, the principle of the method and the algorithms used have been described in detail elsewhere (Ecker and Steiner, 2004).

SPECTRAL IMAGING OF COVID-19 TISSUE

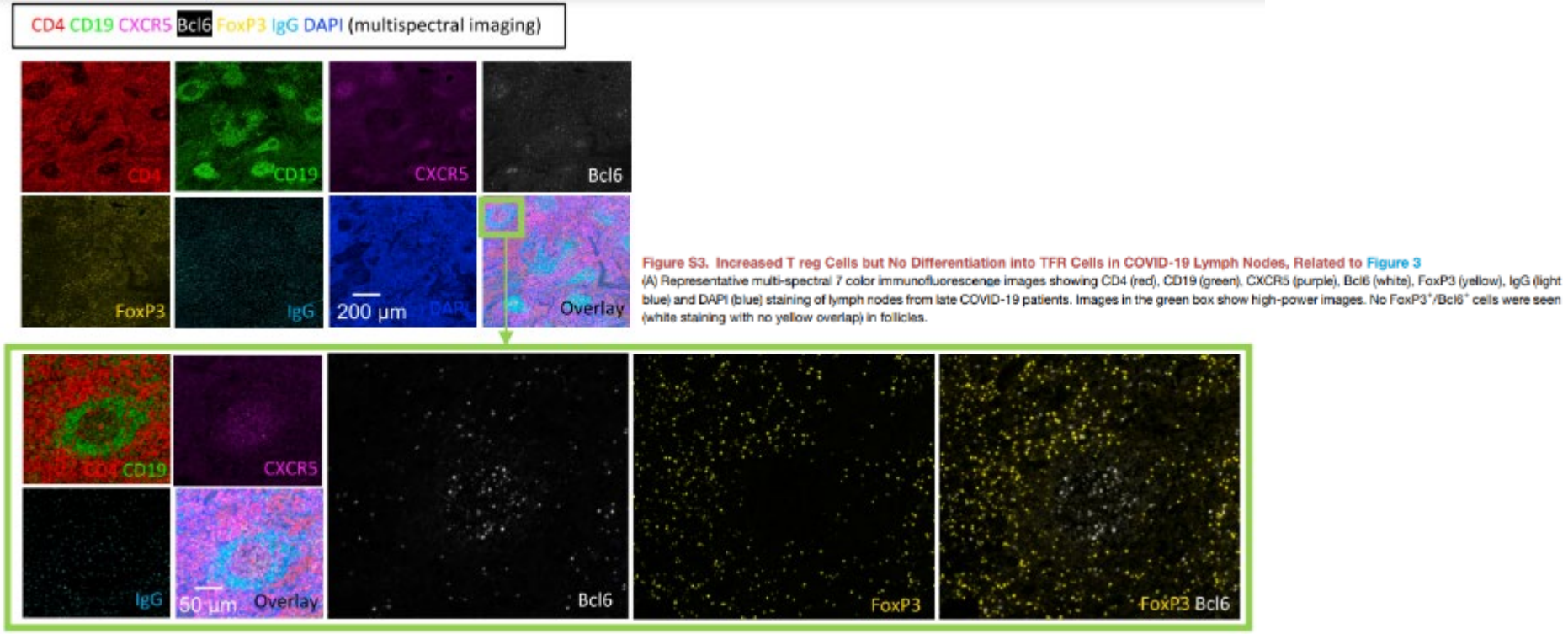

Figure S3. Increased T reg Cells but No Differentiation into TFR Cells in COVID-19 Lymph Nodes, Related to Figure 3

(A) Representative multi-spectral 7 color immunofluorescence images showing CD4 (red), CD19 (green), CXCR5 (purple), Bcl6 (white), FoxP3 (yellow), IgG (light blue) and DAPI (blue) staining of lymph nodes from late COVID-19 patients. Images in the green box show high-power images. No $FoxP3^+/Bcl6^+$ cells were seen (white staining with no yellow overlap) in follicles.

SPECTRAL IMAGING OF COVID-19 TISSUE

Graphical Abstract

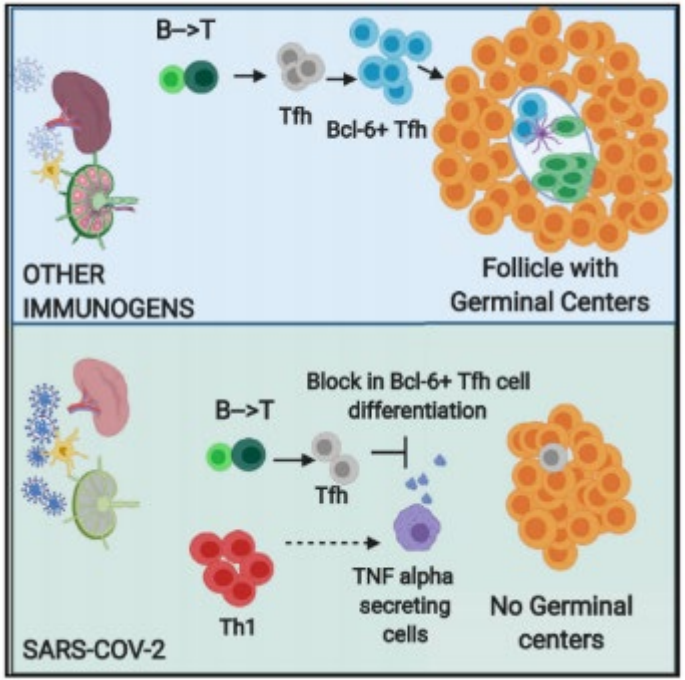

Cell

Loss of Bcl-6-Expressing T Folli and Germinal Centers in COVID

Kaneko et al., 2020, Cell *183*, 1–15
October 1, 2020 © 2020 Elsevier Inc.
https://doi.org/10.1016/j.cell.2020.08.025

Highlights

- Germinal centers are lost in lymph nodes and spleens in acute COVID-19
- Bcl-6$^+$ GC B cells and Bcl-6$^+$ T follicular helper cells are markedly diminished
- Abundant T_{H1} cells and aberrant TNF-α production are seen in COVID-19 lymph nodes
- SARS-CoV-2-specific activated B cells accumulate in the blood of patients

In Brief

Shiv Pillai and colleagues show that in acute COVID-19, there is a striking loss of germinal centers in lymph nodes and spleens and depletion of Bcl-6$^+$ B cells but preservation of AID$^+$ B cells. A specific block in germinal center type Bcl-6$^+$ T follicular helper cell differentiation may explain the loss of germinal centers and the accumulation of non-germinal-center-derived activated B cells. These data suggest an underlying basis for the lower quality and lack of durability of humoral immune responses observed during natural infection with SARS-CoV-2 and have significant implications for expectations of herd immunity.

CONTEXTUAL IMAGE CYTOMETRY

WHERE ARE THE TREGS (CD4+/FOXP3+)?

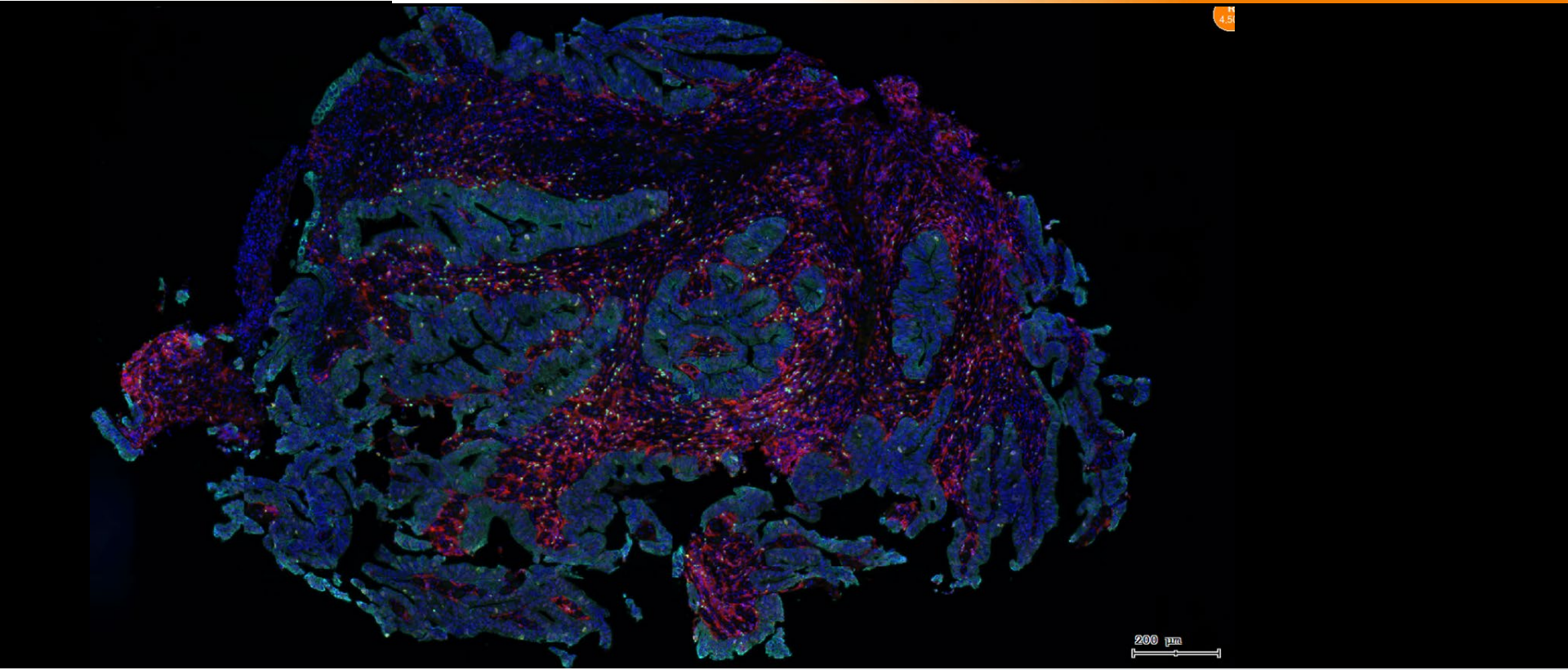

Courtesy Dr. Melanie McCoy, University of Western Australia, Perth

WHERE ARE THE TREGS (CD4+/FOXP3+)?

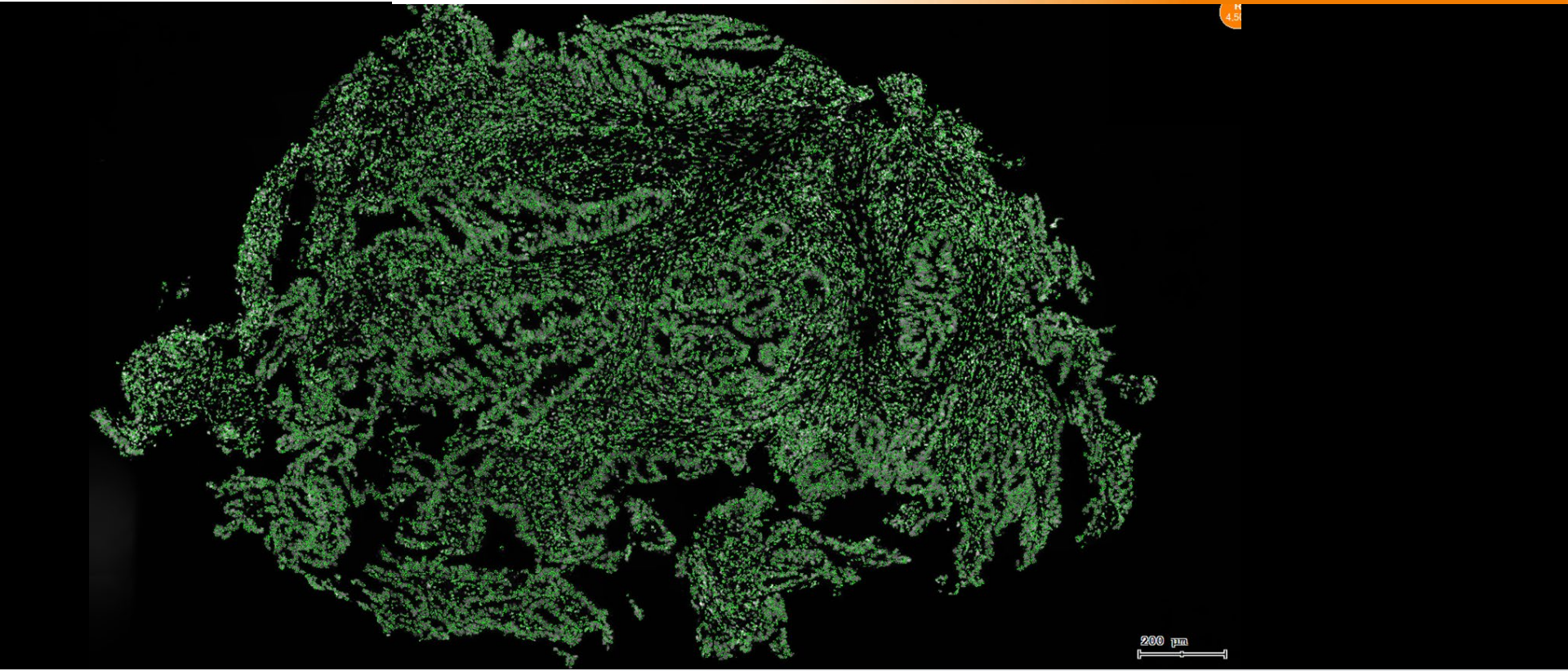

Courtesy Dr. Melanie McCoy, University of Western Australia, Perth

WHERE ARE THE TREGS (CD4+/FOXP3+)?

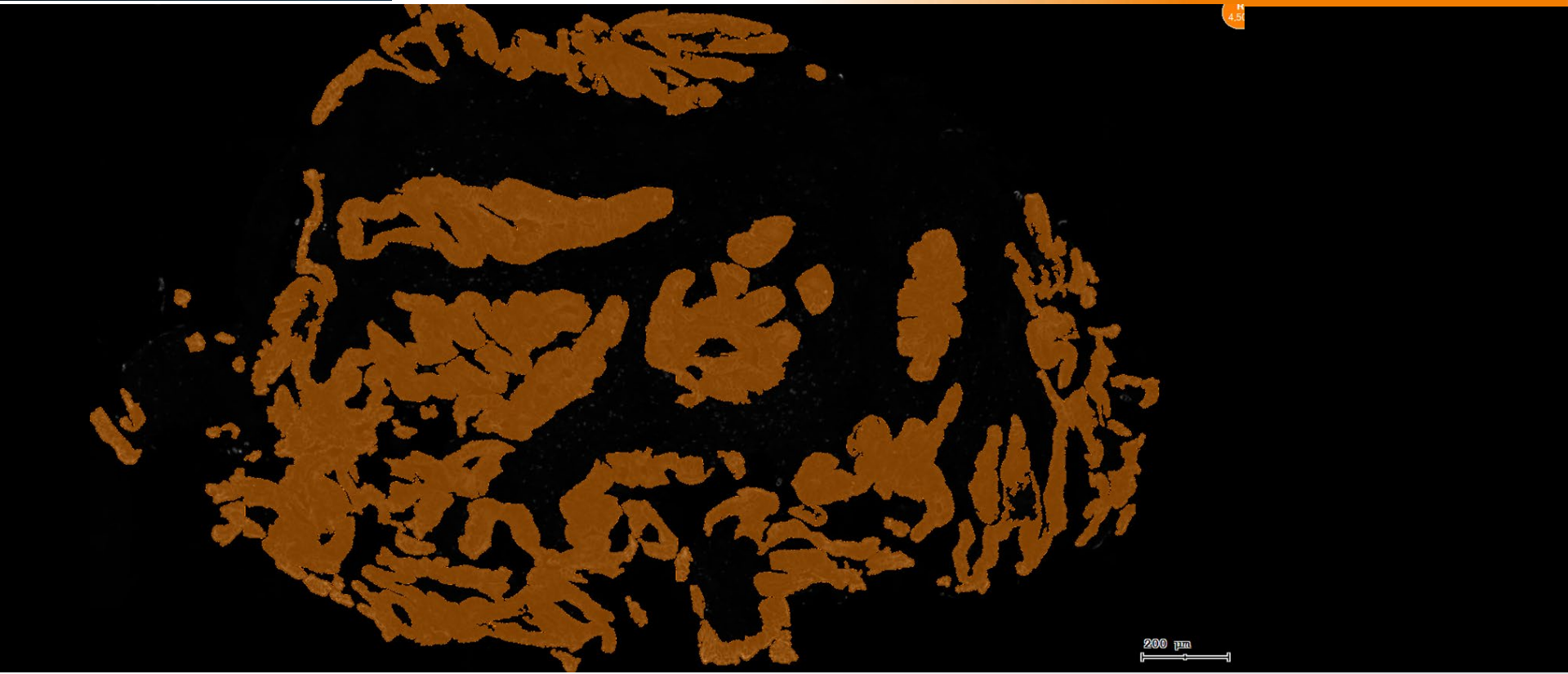

Courtesy Dr. Melanie McCoy, University of Western Australia, Perth

WHERE ARE THE TREGS (CD4+/FOXP3+)?

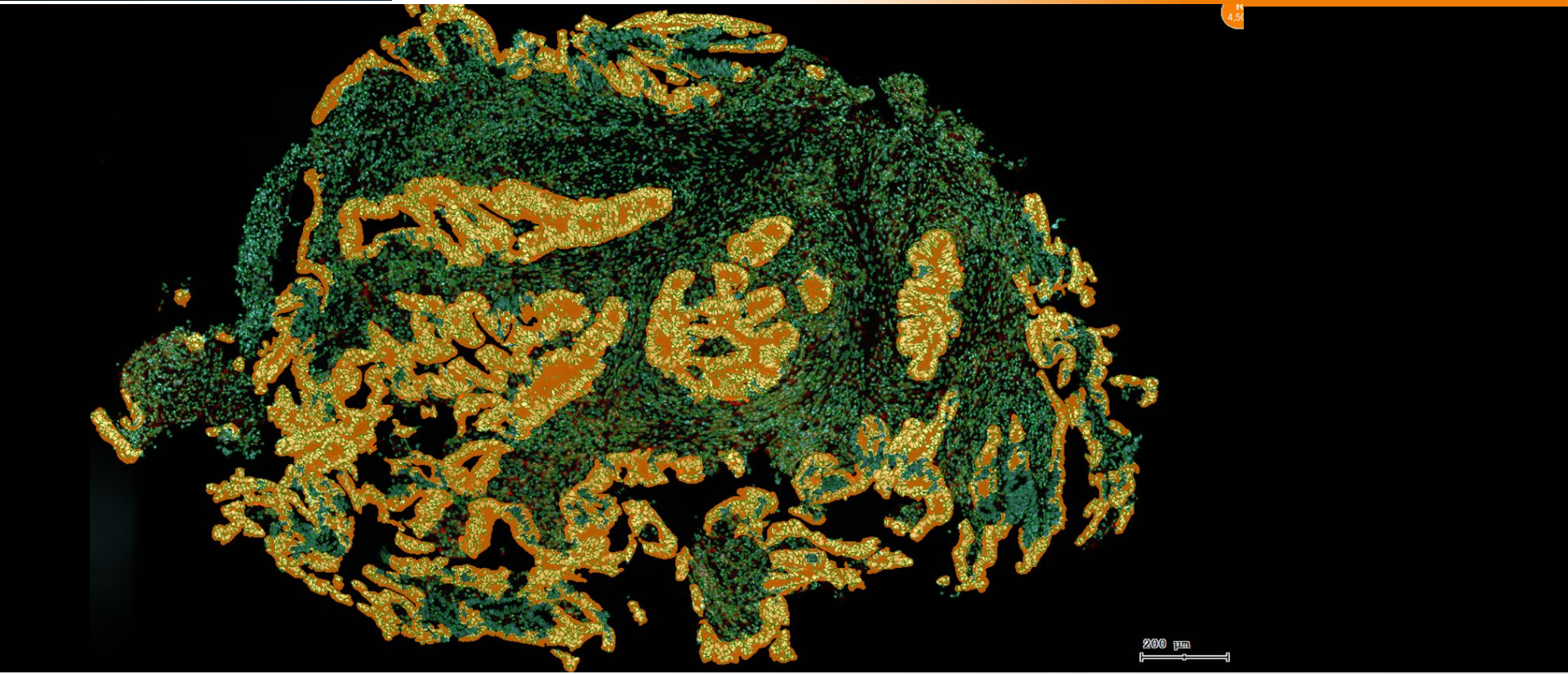

Courtesy Dr. Melanie McCoy, University of Western Australia, Perth

WHERE ARE THE TREGS (CD4+/FOXP3+)?

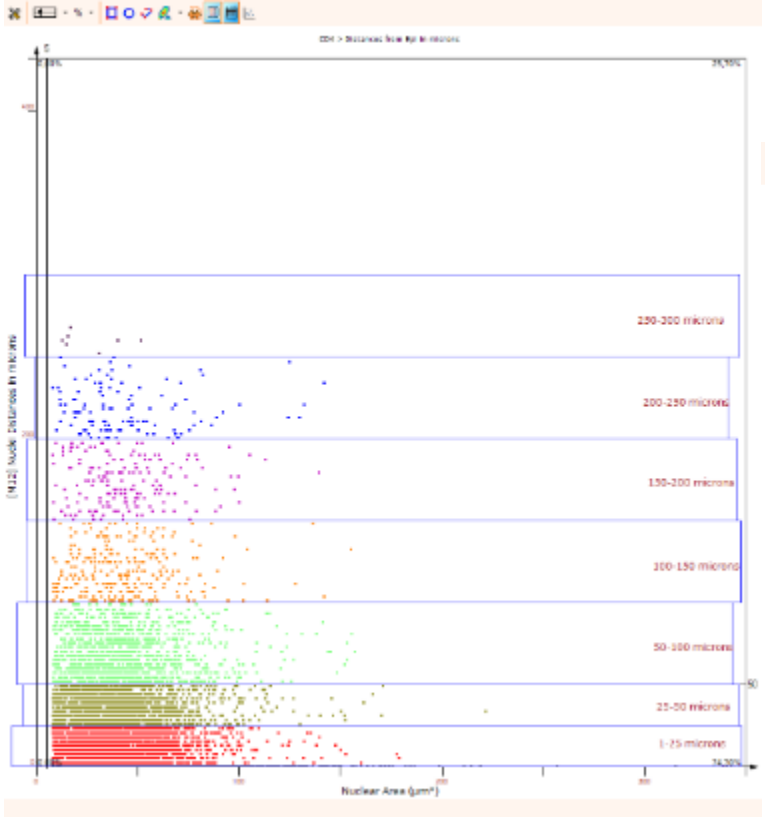

Copy Save Zoo

Statistics

Overall Statistics

Quadrant	Mean of Nuclear Area (µm²)	Mean of [M12] Nuclei Dist...	Count	Percent	No./mm2
UL	0,000	0,000	0	0,00%	0,000
UR	43,442	97,635	1859	25,70%	412,610
LL	0,000	0,000	0	0,00%	0,000
LR	43,787	15,884	5375	74,30%	1192,995
Upper	43,442	97,635	1859	25,70%	412,610
Lower	43,787	15,884	5375	74,30%	1192,995
Left	0,000	0,000	0	0,00%	0,000
Right	43,698	36,893	7234	100,00%	1605,605
Overall	43,698	36,893	7234	100,00%	1605,605
1-25 microns	41,204	11,988	2267	31,34%	503,166
25-50 microns	42,730	36,535	1593	22,02%	353,570
50-100 microns	43,339	69,067	1262	17,45%	280,104
100-150 microns	43,509	119,801	285	3,94%	63,256
150-200 microns	44,311	173,861	184	2,54%	40,839
200-250 microns	44,046	218,078	121	1,67%	26,856
250-300 microns	25,999	260,000	7	0,10%	1,554

Courtesy Dr. Melanie McCoy, University of Western Australia, Perth

WHERE ARE THE TREGS (CD4+/FOXP3+)?

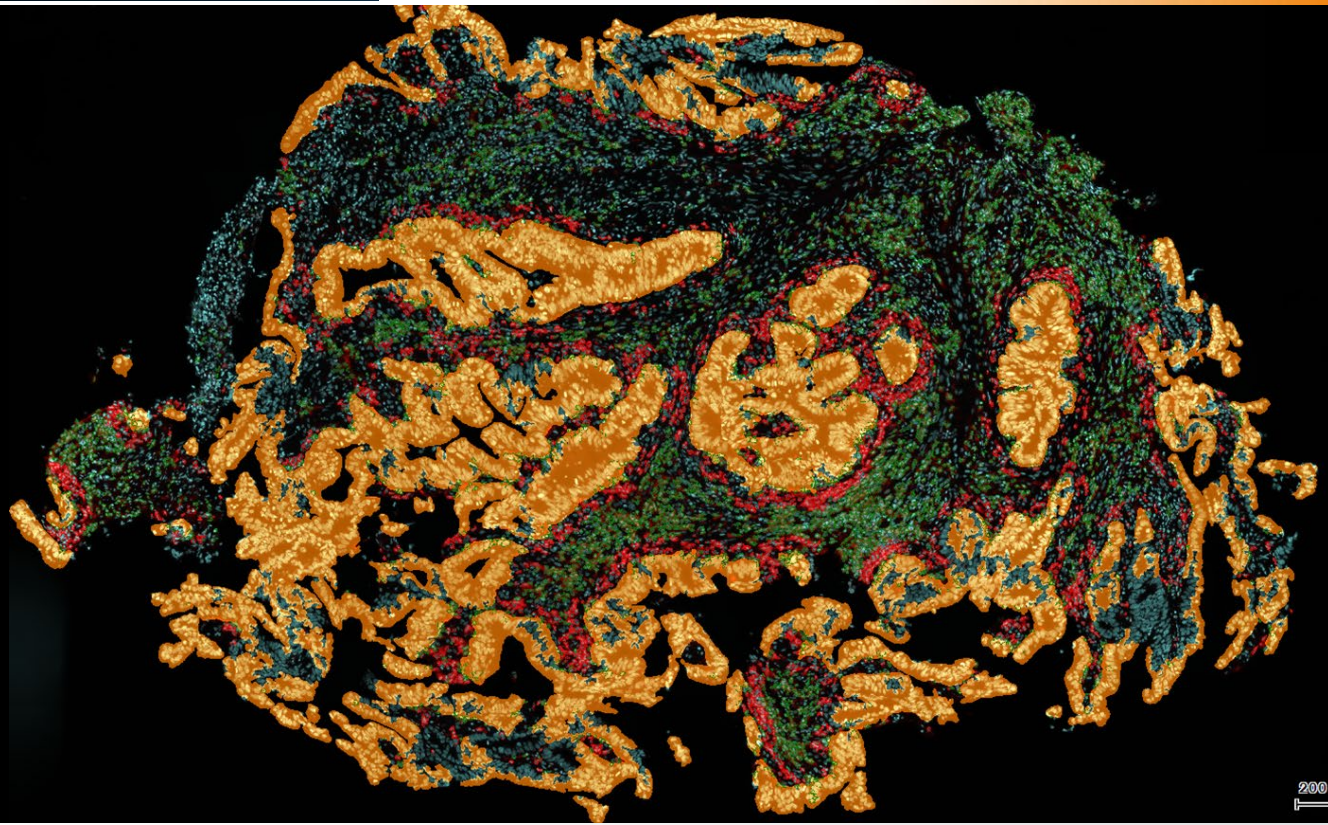

IN RED: CD4+ lymphocytes 1- 25 µm away from next epithelium

Courtesy Dr. Melanie McCoy, University of Western Australia, Perth

WHERE ARE THE TREGS (CD4+/FOXP3+)?

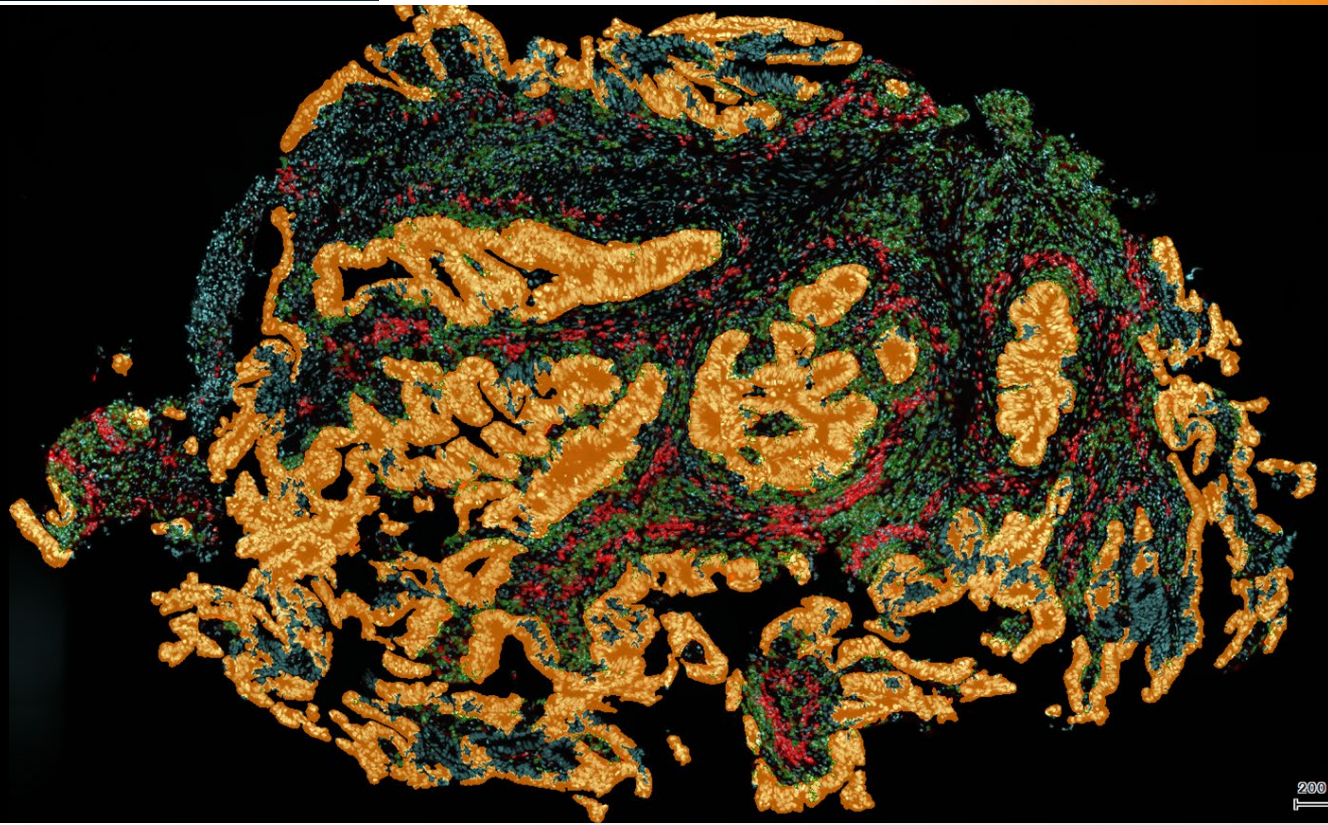

IN RED: CD4+ lymphocytes 25- 50 µm away from next epithelium

Courtesy Dr. Melanie McCoy, University of Western Australia, Perth

WHERE ARE THE TREGS (CD4+/FOXP3+)?

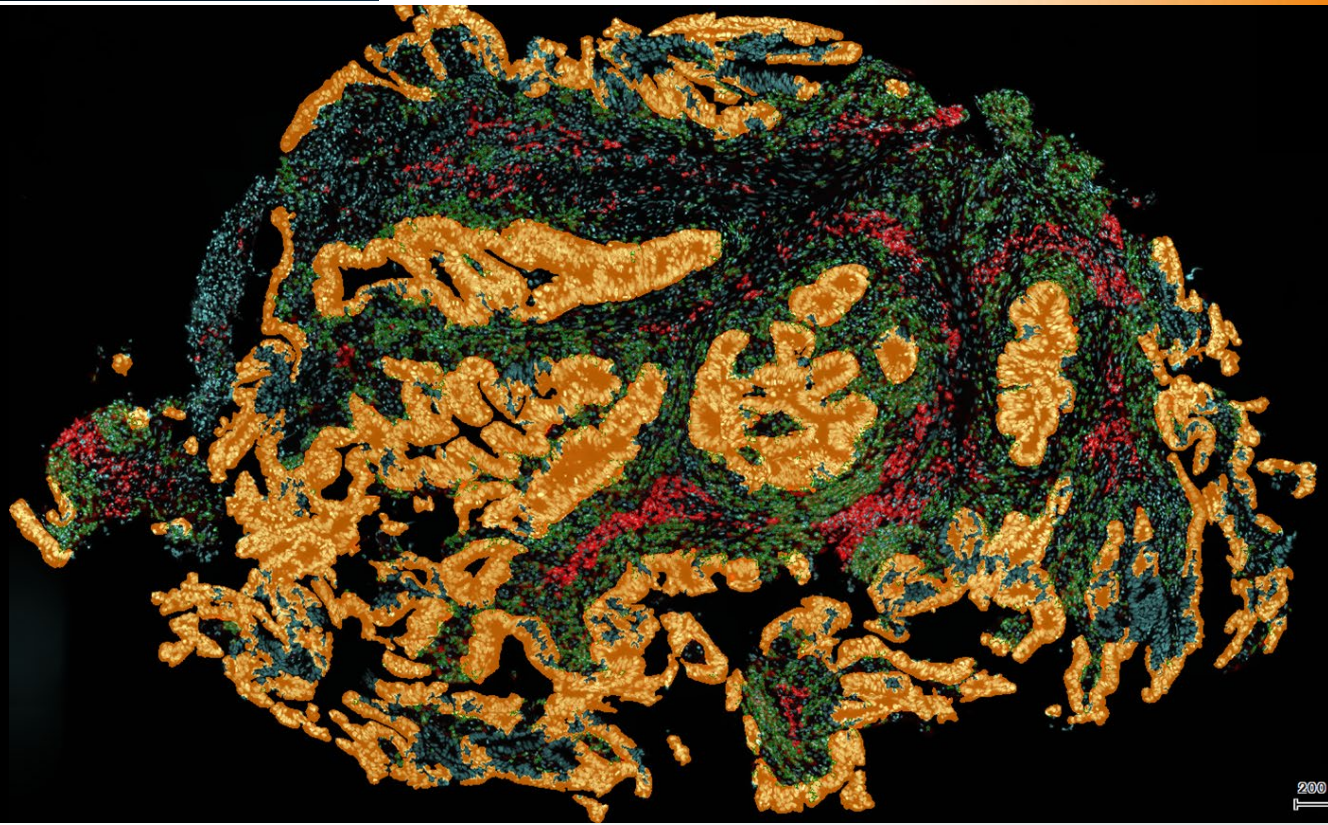

IN RED: CD4+ lymphocytes 50-100 µm away from next epithelium

Courtesy Dr. Melanie McCoy, University of Western Australia, Perth

WHERE ARE THE TREGS (CD4+/FOXP3+)?

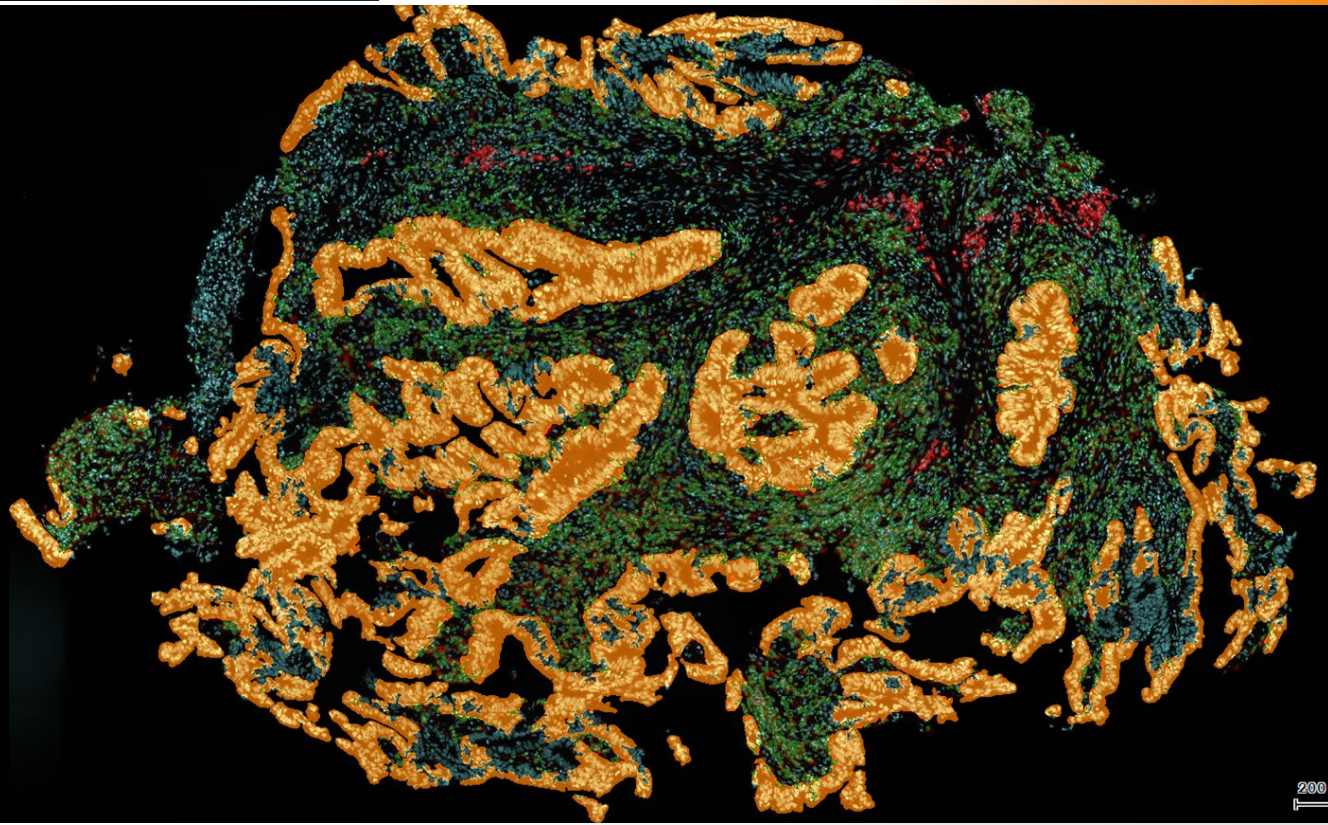

IN RED: CD4+ lymphocytes 100-150 µm away from next epithelium

Courtesy Dr. Melanie McCoy, University of Western Australia, Perth

TUMOR MICROENVIRONMENT
&
SPATIAL PHENOTYPING

DISTRIBUTION OF DIFFERENT T CELLS FROM TUMOR EPITHELIUM

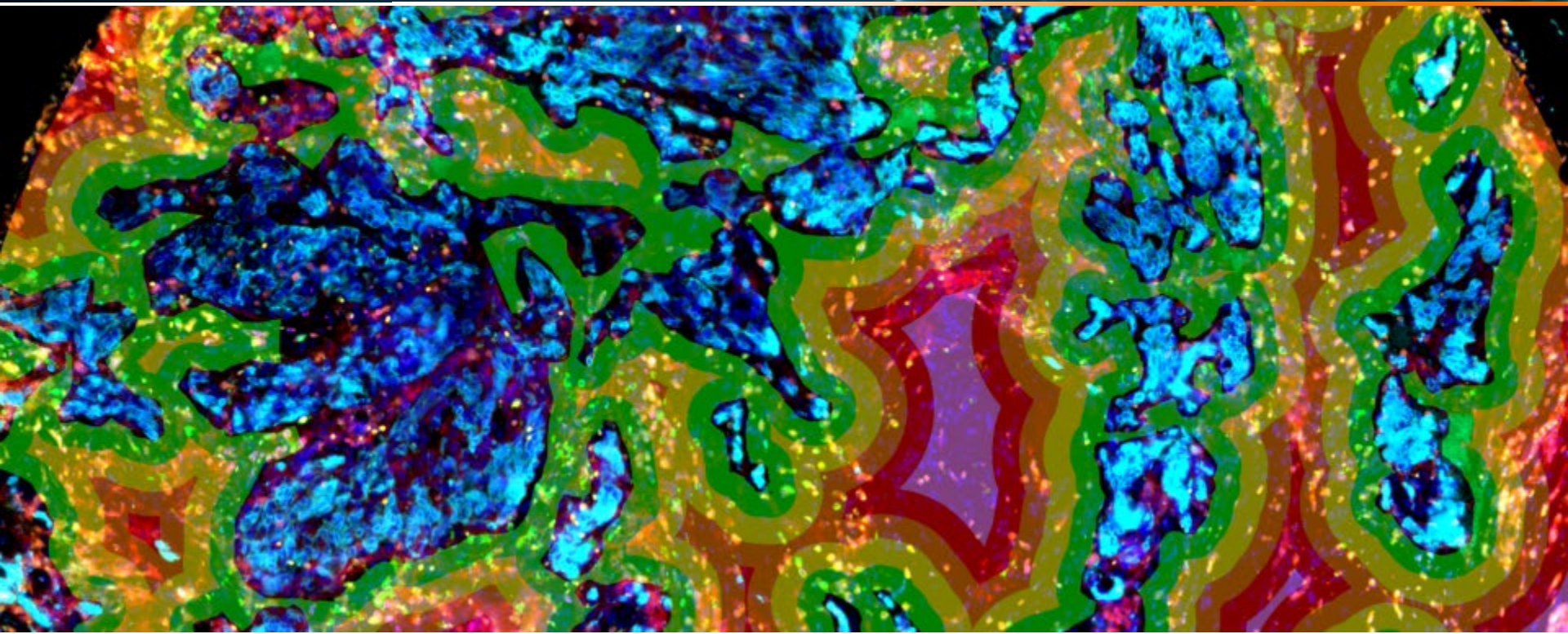

CK+ : Tumor epithelium

Interstitial distance from tumor epithelium : 0-25µm 25-50µm 50-75µm 75-100µm 100-150µm

DISTRIBUTION OF DIFFERENT T CELLS FROM TUMOR EPITHELIUM

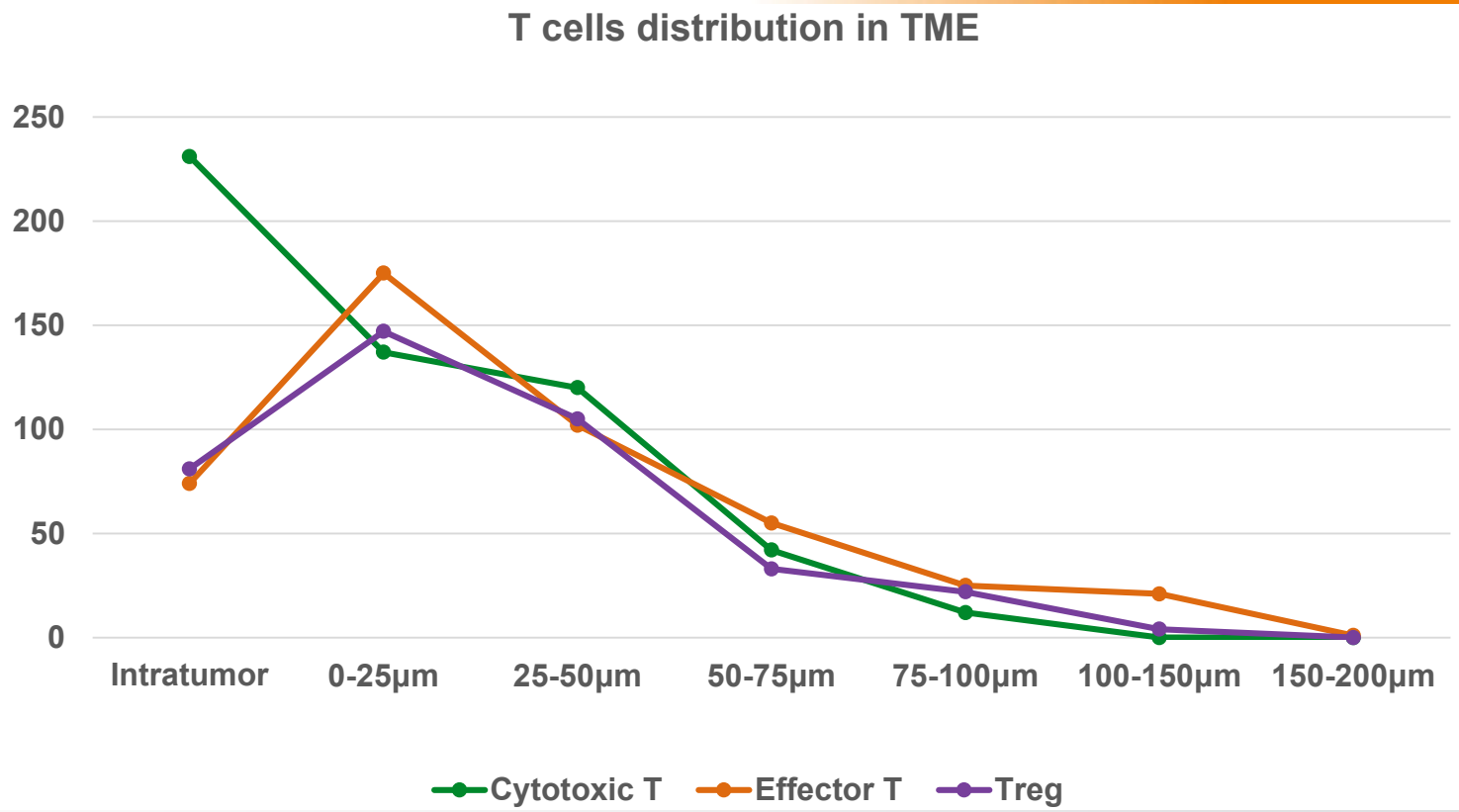

7-CHANNEL SPATIAL PHENOTYPING IN COLON CANCER

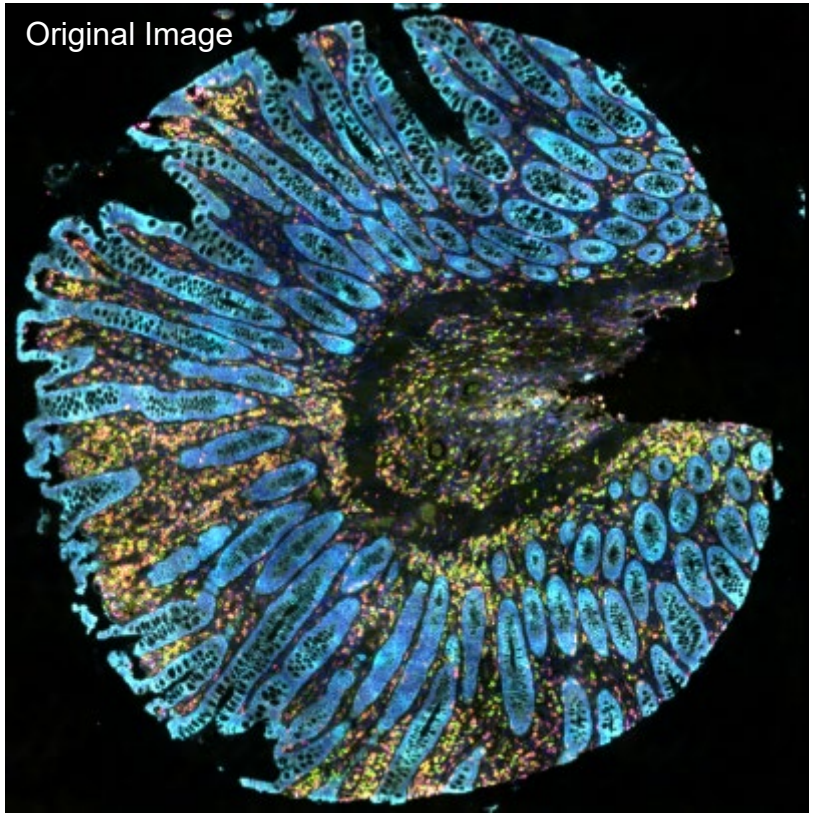

DAPI
CD4
PD-L1
PD1
CD68
CD8
CK

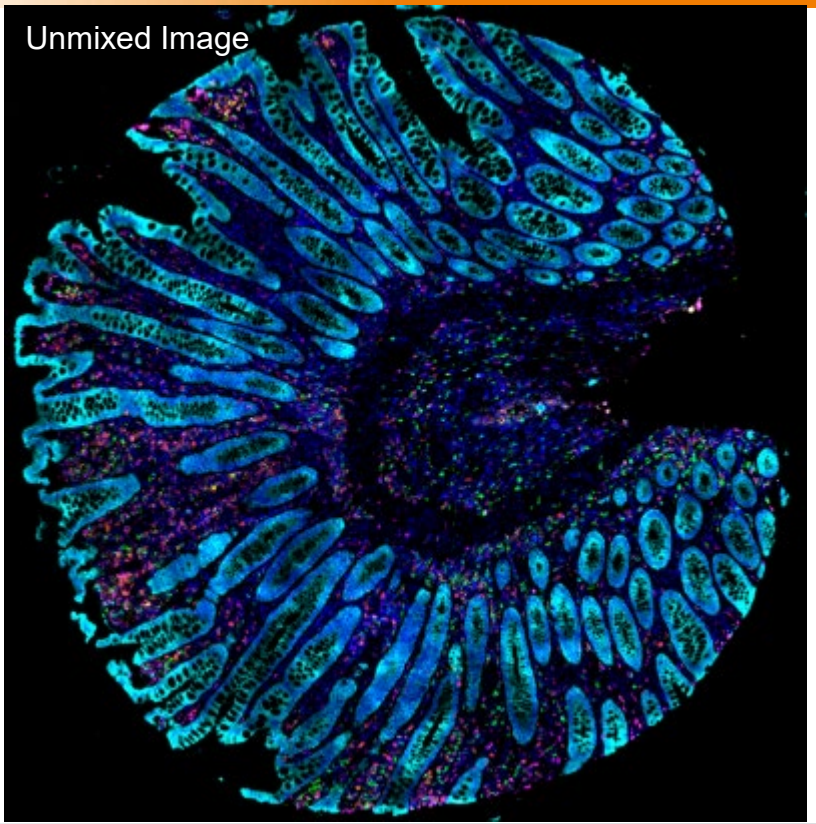

7-CHANNEL SPATIAL PHENOTYPING IN COLON CANCER

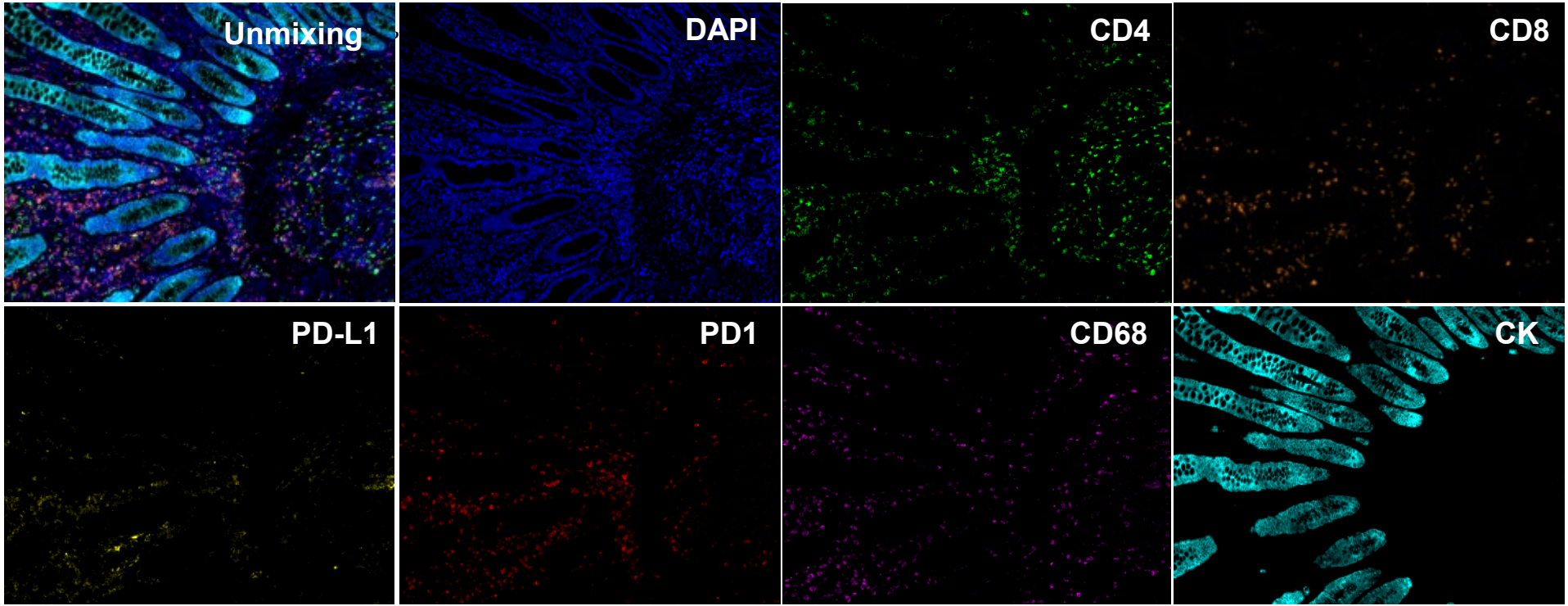

7-CHANNEL SPATIAL PHENOTYPING IN COLON CANCER

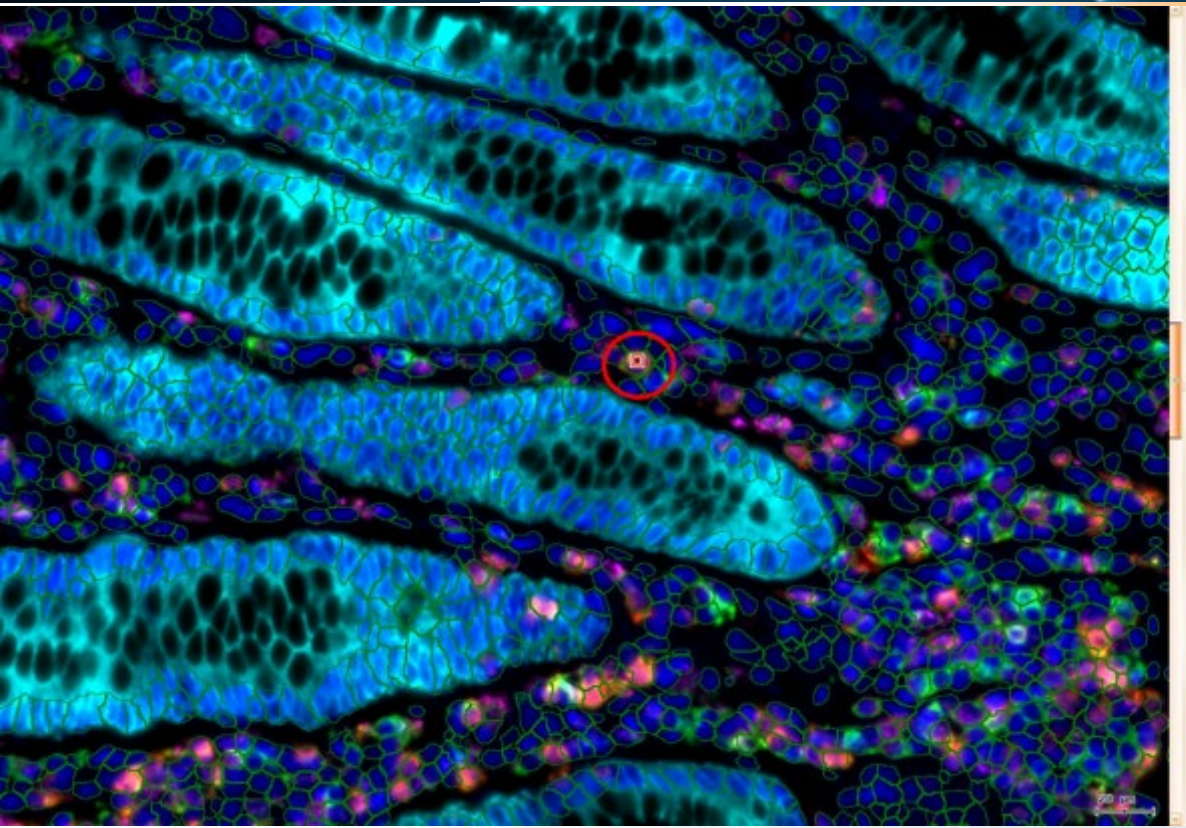

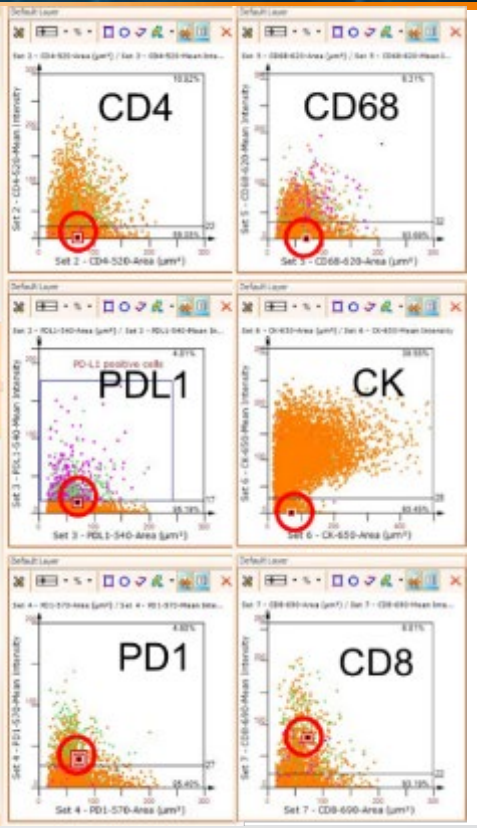

Forward Connection

7-CHANNEL SPATIAL PHENOTYPING IN COLON CANCER

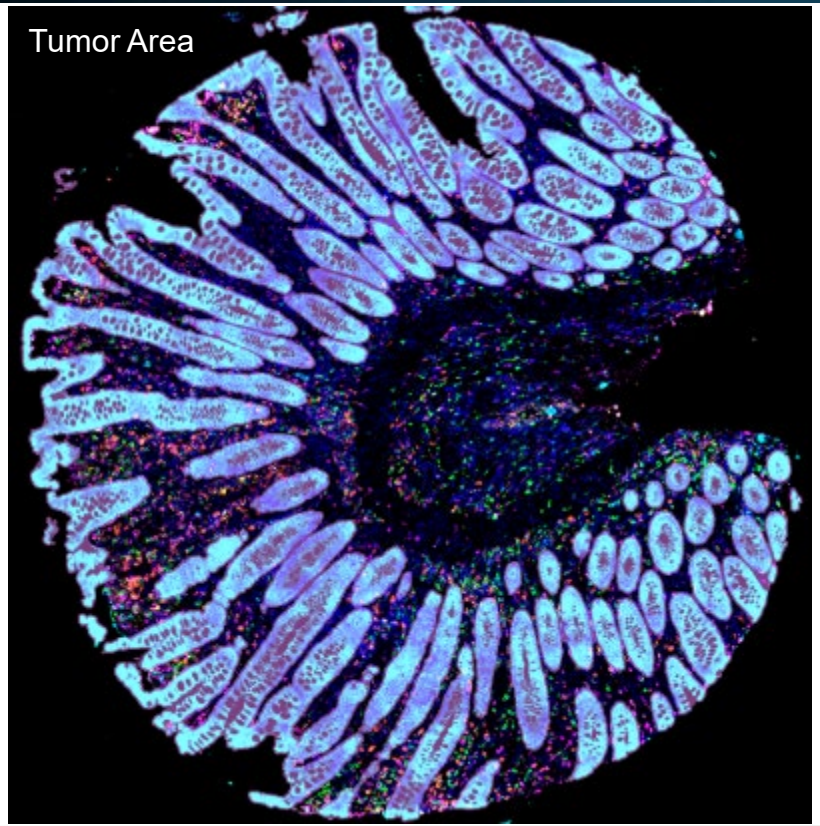

DAPI
CD4
PD-L1
PD1
CD68
CD8
CK

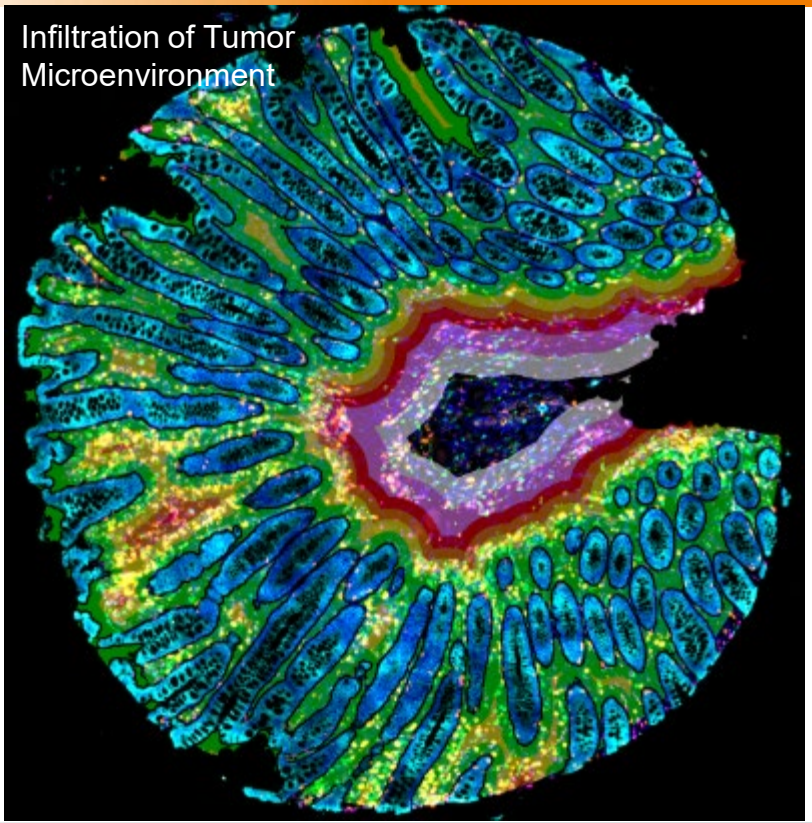

7-CHANNEL SPATIAL PHENOTYPING IN COLON CANCER

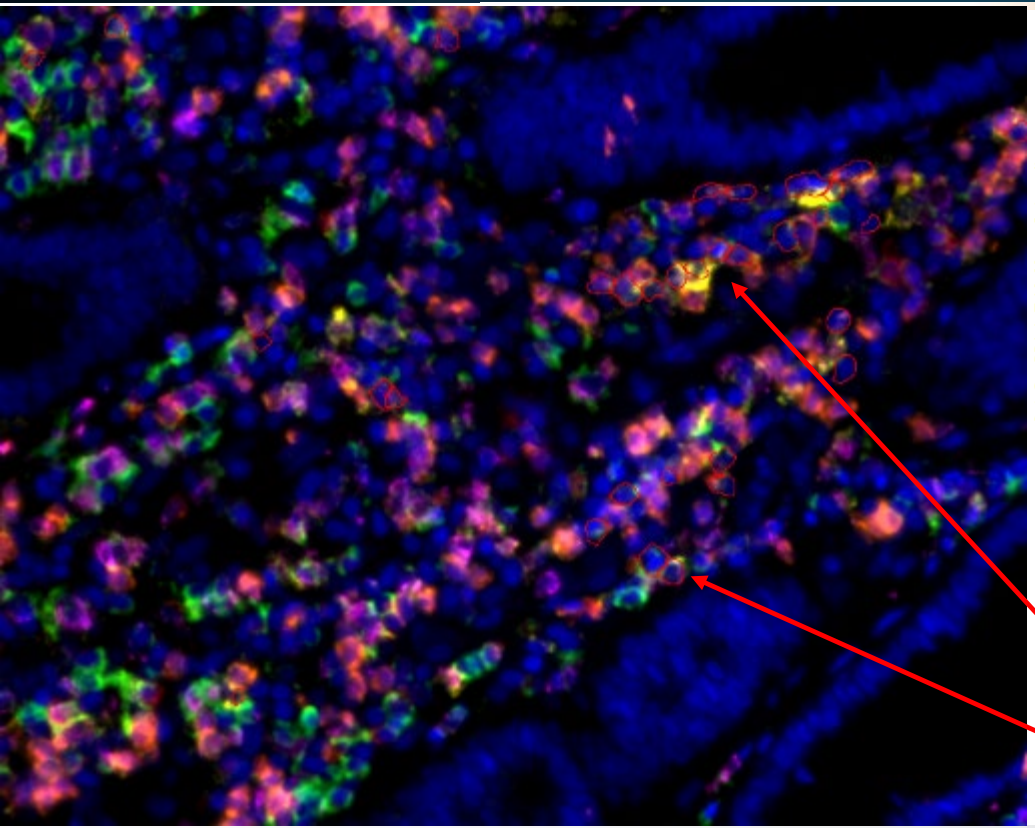

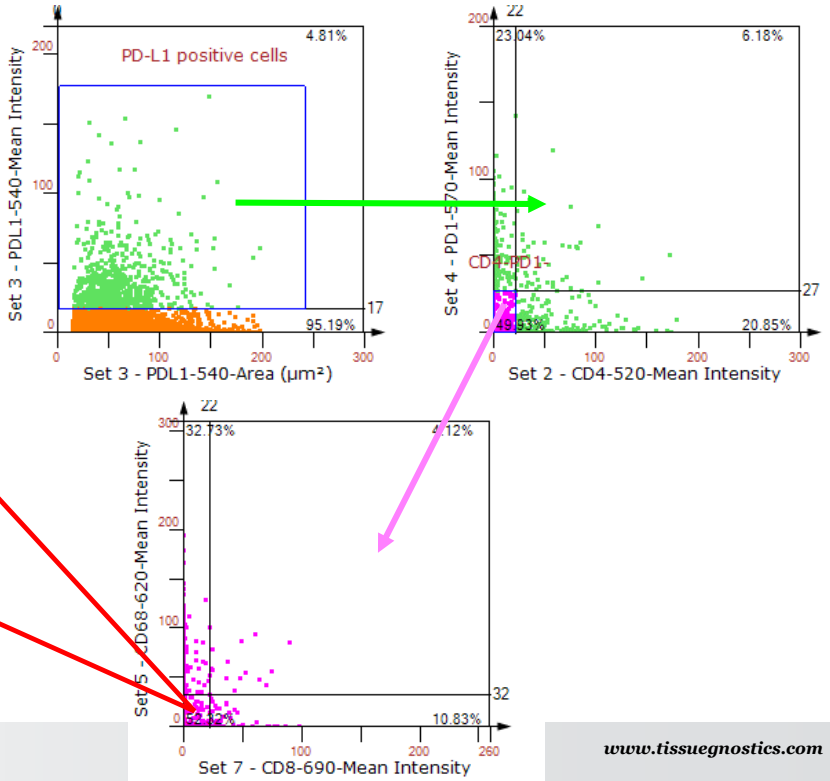

www.impactjournals.com/oncotarget/ Oncotarget, 2017, Vol. 8, (No. 12), pp: 19803-19813

Research Paper

Tumour-infiltrating regulatory T cell density before neoadjuvant chemoradiotherapy for rectal cancer does not predict treatment response

Melanie J. McCoy[1,4], Chris Hemmings[2,3], Chidozie C. Anyaegbu[1], Stephanie J. Austin[1,3], Tracey F. Lee-Pullen[1,3], Timothy J. Miller[1,3], Max K. Bulsara[5], Nikolajs Zeps[1,3], Anna K. Nowak[4,6], Richard A. Lake[4], Cameron F. Platell[1,3]

[1]Colorectal Research Unit, St John of God Subiaco Hospital, Subiaco, WA, 6008, Australia
[2]Department of Anatomic Pathology, St John of God Pathology, Wembley, WA, 6014, Australia
[3]School of Surgery, University of Western Australia, Crawley, WA, 6009, Australia
[4]School of Medicine and Pharmacology, University of Western Australia, Crawley, WA, 6009, Australia
[5]Institute for Health Research, University of Notre Dame, Fremantle, WA, 6959, Australia
[6]Department of Medical Oncology, Sir Charles Gairdner Hospital, Nedlands, WA, 6009, Australia

Correspondence to: *Melanie McCoy,* ***email:*** *melanie.mccoy@uwa.edu.au*

Keywords: *rectal cancer, regulatory T cells, radiotherapy, chemotherapy, treatment response*
Received: *September 13, 2016* ***Accepted:*** *January 07, 2017* ***Published:*** *February 03, 2017*

www.impactjournals.com/oncotarget/ Oncotarget, Supplementary Materials 2017

A

	Visual Counts				Automated count
	Observer 1	Observer 2	Observer 3	Median	(DAB Nuclear Segmentation)
ROI 02	17	20	18	18	20
ROI 04	25	29	28	28	26
ROI 01	30	34	33	33	34
ROI 03	44	52	42	44	48
ROI 06	49	52	46	49	54
ROI 05	43	56	51	51	55
ROI 09	53	51	49	51	53
ROI 10	59	68	55	59	63
ROI 08	228	220	212	220	236
ROI 07	256	325	296	296	433

B

	Observer 1	Observer 2	Observer 3	Median	Automated
Observer 1		0.888**	0.927***	0.948***	0.915***
Observer 2	0.888**		0.960***	0.945***	0.979***
Observer 3	0.927***	0.960***		0.997***	0.988***
Median	0.948***	0.945***	0.997***		0.979***
Automated	0.915**	0.979***	0.988***	0.979***	

Supplementary Figure 3: Visual versus automated Foxp3⁺ cell counts. Ten regions of interest (ROI; mean area 0.88 mm²) were selected on the digital images from five different patients. Regions were selected to represent a range in Foxp3⁺ cell densities, as determined by eye. The number of Foxp3⁺ cells was counted by three independent observers and the regions were then subjected to automated image analysis using StrataQuest version 5 (TissueGnostics, Taborstraße, Vienna, Austria), using our optimised analysis profile based on DAB nuclear staining segmentation. **A.** Number of Foxp3⁺ cells per ROI, ordered by increasing Foxp3⁺ cell density according to the median visual count. **B.** Spearman correlation coefficient for each pair-wise comparison; ** $p < 0.01$, *** $p < 0.001$.

REPRODUCIBILITY & STANDARDIZATION

TissueFAXS Cytometry supports researchers to move

FROM IMAGE TO DATA

and increase observer independence & reproducibility!

rupert.ecker@tissuegnostics.com

TISSUEGNOSTICS